# Phyllotaxis: a remarkable example of developmental canalization in plants

Christophe Godin, Christophe Golé, Stéphane Douady

# Phyllotaxis: a remarkable example of developmental canalization in plants

Christophe Godin, Christophe Golé, Stéphane Douady

September 2019

## Abstract

Why living forms develop in a relatively robust manner, despite various sources of internal or external variability, is a fundamental question in developmental biology. Part of the answer relies on the notion of developmental constraints: at any stage of ontogenenesis, morphogenetic processes are constrained to operate within the context of the current organism being built, which is thought to bias or to limit phenotype variability. One universal aspect of this context is the shape of the organism itself that progressively channels the development of the organism toward its final shape. Here, we illustrate this notion with plants, where conspicuous patterns are formed by the lateral organs produced by apical meristems. These patterns, called phyllotaxis, traditionally fall into two broad categories, spiral or whorled that present striking symmetries and regularities. These properties suggest that plant development is strongly canalized and cannot escape specific attraction patterns. Since the early 19th century, researchers have looked for biological or physical explanations for such amazing and specific form "attractors". Thanks to this collective and sustained effort, we now have gained much insight on this self-organizing process, and uncovered important parts of the mystery. This paper aims to provide an easy-to-read overview of the main concepts that have been developed to explain phyllotaxis and to make clear their connections in a step-by-step progression, while keeping the mathematics light. We suggest that altogether a view emerges where phyllotaxis appears as a remarkable example of how shapes may be canalized during development.

## 1    Introduction

In developmental biology, the notion of developmental constraints refers to the idea that at every stage of ontogenesis, morphogenetic processes are constrained by the current chemical, and physical, state of the organism (Alberch 1982, 1991), which biases or limits phenotype variability (Maynard Smith et al. 1985). At each stage of the development, these constraints progressively restrict the set of possible shapes that can be achieved by the organism. In this way, during ontogenesis, developmental constraints may canalize the development of an organism in a very narrow region of the morphospace. Such canalization of shapes is believed to be one major source of shape reproducibility in both animals and plants, by making shape development insensitive to external or internal variations of moderate amplitudes (Maynard Smith et al. 1985, Félix & Barkoulas 2015, Debat & Le Rouzic 2019).

The spiral arrangement of organs on plant stems, called spiral phyllotaxis, is a striking example of phenotypic bias in development. A vast majority of these spiral patterns tend to show numbers of spirals that are numbers in the sequence:

$$1, 1, 2, 3, 5, 8, 13, 21, 34, 55, 89, 144, \cdots$$

known as Fibonacci's sequence. This phenomenon is sometimes referred to as *numerical canalization* (Huether 1968, Vlot & Bachmann 1991, Battjes et al. 1993).

In this paper, we show in a step by step manner how the robust and conspicuous spiral phyllotaxis patterns, are actually channeled by purely geometric developmental constraints throughout plant development. We provide a detailed account of the origin of these constraints, appearing in models assuming only purely local interaction rules, and discuss the consequences of such a mechanism of plant patterning.

For this, we first briefly recall concepts that have been developed about phyllotaxis. We start with the fascinating mathematical properties associated with the Fibonacci sequence (section 2). We then explain in a geometrically intuitive manner the main origin of these mathematical properties (section 3) and analyze the dynamical mechanisms that have been proposed in the literature, based on local interaction rules between organs (Section 5). In this view, the competition for space in the shoot apical meristem (SAM), spanning the plant's entire life, imposes simple, local and robust geometric rules on the shape of the evolving morphogenetic front of newly formed organs around the SAM. These rules can explain both the universal presence of Fibonacci phyllotaxis in plant patterns and its exceptions, depending on the variation of the growth rate parameters. This suggests that phyllotaxis patterns are actually continuously canalized during plant development (section 6).

# 2 Regular phyllotaxis patterns and their mathematics

Phyllotaxis patterns are usually classified into either spiral or whorled motifs according to the number of lateral organs attached at each node (Fig. 1.A-B). In the large class of spiral phyllotaxis on which we focus in this paper, the patterns can usually be described by two families of visual spirals, turning in opposite directions: the parastichies (Fig. 1.C). As early as at the beginning of the $19^{th}$ century (Braun 1831), it was recognized that, surprisingly, the numbers of spirals of these clockwise and anticlockwise families are in general exactly two consecutive numbers of the Fibonacci sequence where each term, beyond the first two 1's at the beginning, results from the sum of the two preceding ones (see Box 1). This pair of numbers is called the phyllotaxis mode. For some genus, like certain *Dipsacus*, the mode comes as a multiple of Fibonacci numbers. Quite unusual for a biological system, these numbers of spirals show only marginal deviation from this rule (around few percents) (Fierz 2015, Swinton et al. 2016), suggesting the existence of a strong and relatively universal developmental constraint (Maynard Smith et al. 1985).

The organs are initiated in a small structure at the tip of plant axes, called the shoot apical meristem (SAM) (Fig. 2.A) that produces organs at a regular pace at the rim of a central zone (CZ) where no organ can form. The organs then grow and extend to reach their final size and shape. During this process they essentially keep their relative positions. The angle between two consecutive organ primordia is called the *divergence angle* (Fig. 2.B-C) (Schimper 1835). In most plants this angle does not change as the primordia develop and become mature organs. Divergence angles may be relatively constant during some growth phase of the stem or to the contrary show gradual variations. The imaginary curve linking the organs at consecutive nodes of a given stem (in the order of their initiation) is called the *generative spiral* (Fig. 2.B-C). It can be seen as the most horizontal possible spiral winding around the stem and which traverses each organ in their chronological order. This spiral winds either to the left or to the right (chirality).

When no twist occurs on the stem, the divergence angle can easily be observed on elongated stems. Using microscopes, it can as well be observed directly in the SAM with some additional
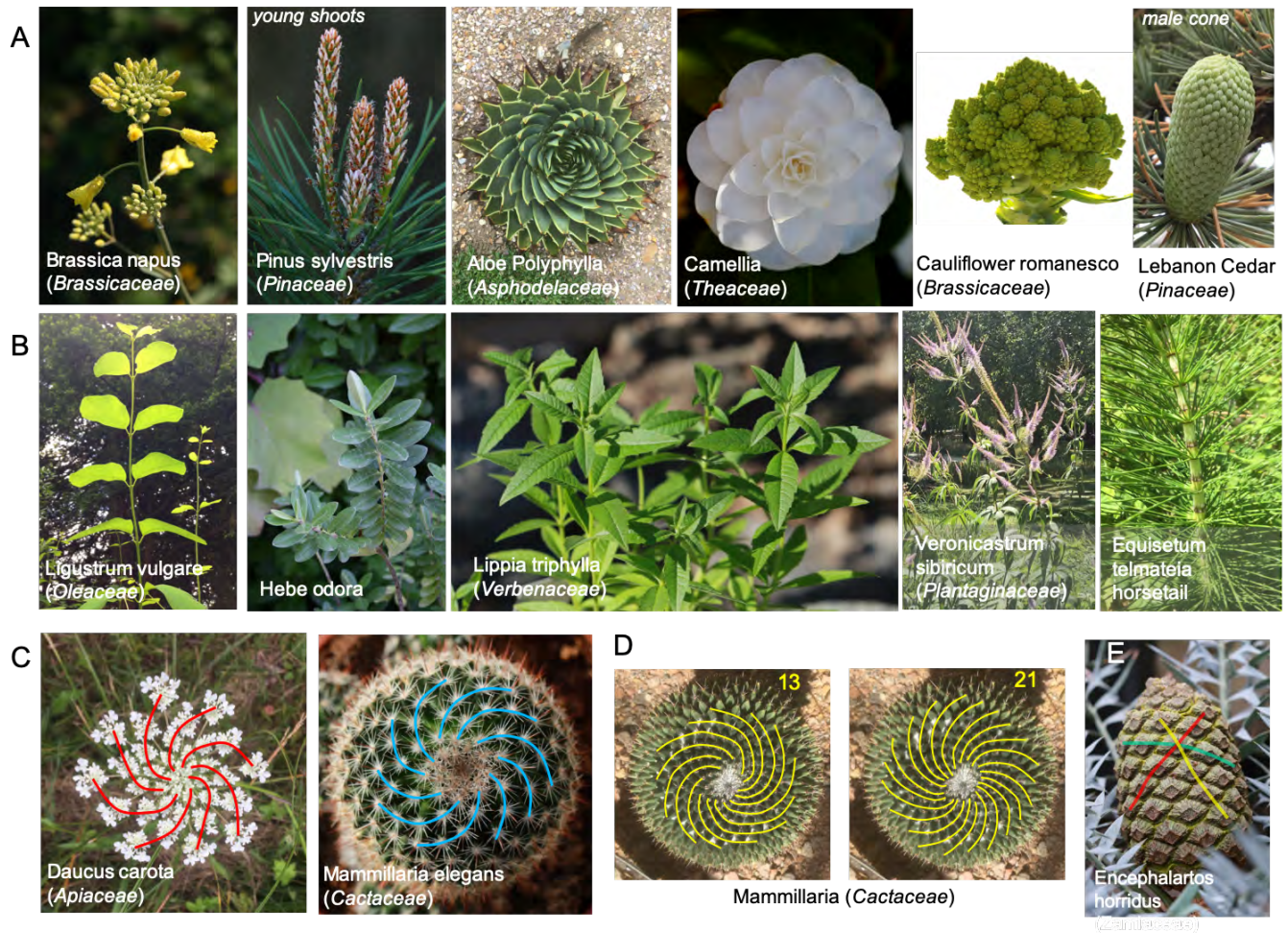
Figure 1: **Phyllotaxis patterns in a nutshell.** (A) Examples of spiral phyllotaxis (1 organ per node) on different plant parts. (B) Whorled phyllotaxis (more than one organ per node). (C) Individual spirals making up a spiral pattern are called parastichies. (D) Parastichies come generally in two (or three) families of spirals: clockwise and counter-clockwise. These pairs of parastichy numbers are most of the time consecutive numbers in the Fibonacci sequence (E) A third more vertical family sometimes clearly appears (orthostichy) like in pine apple or on the fruit of Encephalortos horribus for example.

efforts. On elongated stems, its average value can easily be estimated from the count of the leaves between two leaves overlaying in their azimuthal orientation and the number of turns to get from one to the other following the generative spiral (Fig. 2.C) (Schimper 1835). In contrast, a similar strategy is not possible in compact structures such as flowers as one cannot count as easily the number of turns between two overlaying organs and the number of organs between them. Rather, one observes a certain number of conspicuous spirals connecting organs in contact, turning in one or the other direction. These conspicuous spirals (or parastichies) that one sees on many plants must not be confused with the generative spiral. They stem from the spatial adjacency between organs when the structure remains compact, such as in cones or inflorescences (Fig. 2.D)(Braun 1831, Bravais & Bravais 1837): in general, organs do not exactly overlay (Fig. 2.C) and if the structure remains compact, one can observe the corresponding slight shift on one side (Fig. 2.D left). Through development, this shift always occurs in the same direction, which creates the different visual spirals (Fig. 2.D right, Fig.1.E). For spiral phyllotaxis, the average divergence angle (when it can be measured) is most of the time close to the golden angle (137.5°) (Fig 2.B) while other angles such as 99.5° (Lucas angle) can be found but are much less frequent (Fierz 2015, Swinton et al. 2016). Remarkably, both the golden angle and Lucas angle are tightly connected with the Fibonacci sequence (Box 1), which adds to the intuition that something profound must connect these botanical patterns, and their resilience to internal, environmental, and genetic variations, to mathematics.

Both numbers of parastichies and divergence angles thus seem to be constrained to take their values within very restricted ranges. Where do these developmental constraints come from? Do they reflect a single underlying mechanism, acting on the parastichy numbers, or the divergence angle? or are two different mechanisms at play?

# 3   The geometric link between divergence angle and spirals

To better understand the intricate relationship between divergence angle and parastichies, let us consider a very simple geometric model of organ initiation (Fig. 3.A). In the model, organs (orange dots) form, one at a time, at the rim of the meristem central zone (green disk of radius $R$). The laps of time between two consecutive organ initiation, $T$, is called a plastochrone and the azimuthal angle, $\alpha$, between these organs defines the divergence angle. As soon as they are produced, the organs move radially away from the center with a constant velocity $V$. We make the simplifying assumption that apex growth is regular (stationary growth), so that $V$, $T$, and $\alpha$, are considered as independent and constant parameters. For sake of notation simplicity, we will measure angles as fractions of a circle: any angle will be represented by a real number between 0 and 1 (the angle unit is *a turn, e.g.* $1/2 = 180°, 1/3 = 120°, 1/4 = 90°\dots$).

**First connection between divergence angle and spiral motifs.**   Using this model[1]. we can simulate the growth of an apex during a given number of plastochrones (at least 50 in our pictures). Let us first observe what happens when we vary the divergence angle ($\alpha$ stays constant during each simulation but is distinct between two simulations, while $R = 1$ and $V = 1$ in arbitrary units (a.u.) are fixed and common to all simulations). For $\alpha = 1/2$, the model generates two opposite straight arms at 180° of one another. The primordia are generated alternatively on each side, left and right, and move away from the center, thus leaving room for the next primordium on the same side every two plastochrones. The two arms are thus composed respectively of even and odd primordia. This disposition is observed commonly in plants and is

---

[1]The interested reader might want to manipulate the model using our interactive online geogebra app *Archimedean spirals*
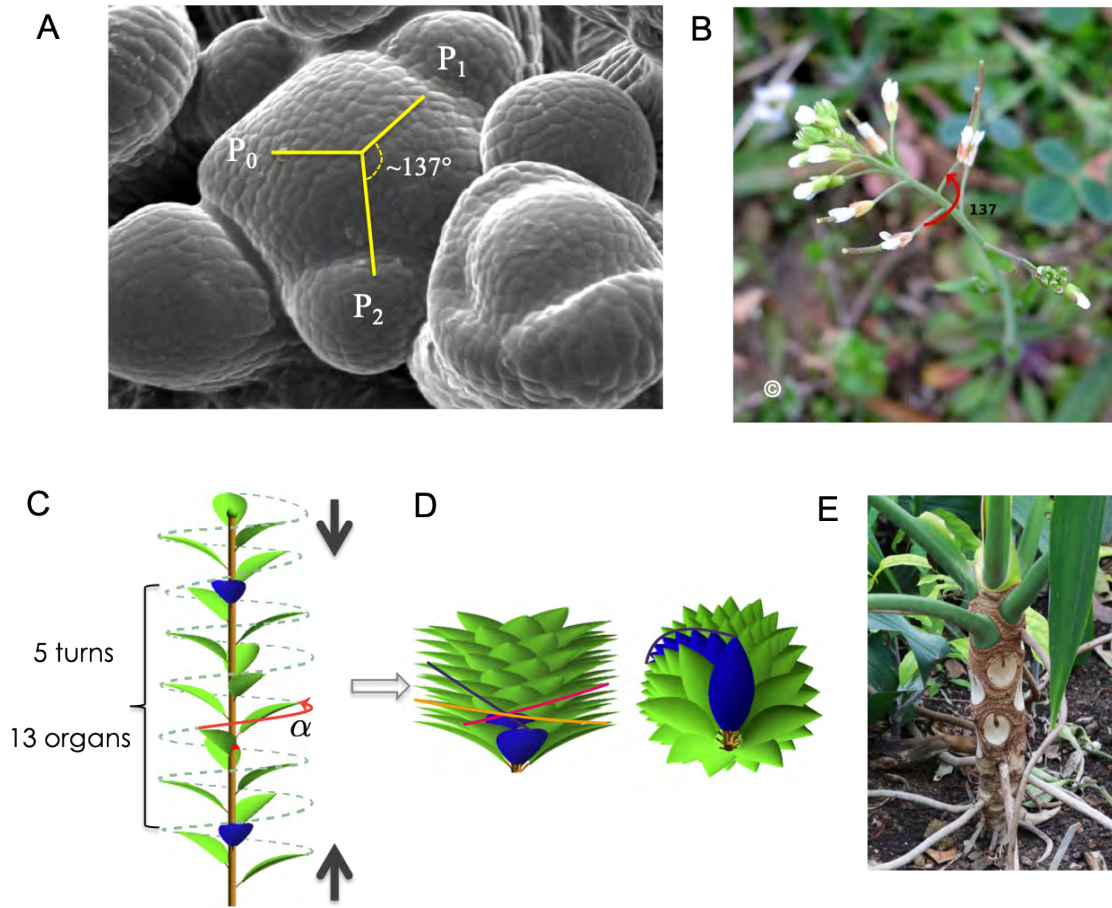
Figure 2: **Where do spirals come from ?** (A) The meristem: the organ factory (here floral meristem of Arabidopsis thaliana, photo courtesy of Jan Traas). Organ are generated in sequence at precise positions on the flank of the meristem separated by a relatively constant divergence angle. (B) In general, the divergence angle remains unchanged after internode elongation (here Inflorescence of Arabidopsis thaliana). (C) The spiral made by the imaginary curve joining the consecutive organs is called the generative spiral. If one considers a pair of leaves with similar orientation on the stem (colored in blue), it is easy to estimate the average divergence angle separating these two leaves: mean divergence angle = #turns / #organs = 5/13 = 0.385 turn = 138.5°. (D) If we (virtually) contract this structure, the leaves that are in the same direction get visually close to each other. In many cases they do not exactly overlay and present actually a small angular deviation. This deviation spreads along the contracted structure and generates visually spirals. (E) Similar spirals can be observed on leaf scars on plant stems.
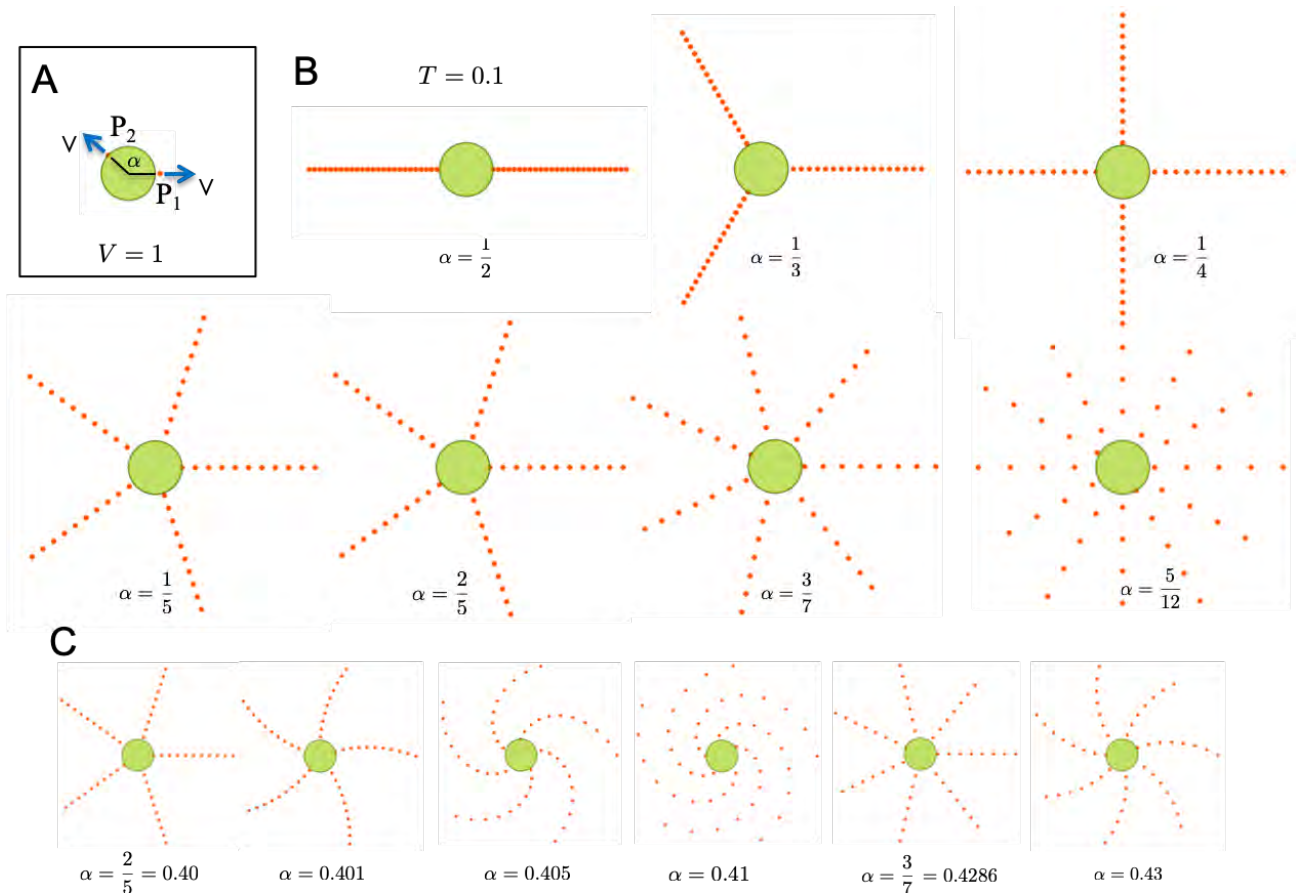
Figure 3: **Testing the relation between divergence angle and emerging phyllotaxis motifs using a simple kinematic model.** (A) Simple kinematic model: Organs (orange dots) are initiated at the periphery of the central zone (green disk). Primordia are initiated with a constant period $T$ during the simulation and move radially away from the center at a constant velocity $V = 1.0$ arbitrary length unit / arbitrary time unit. The value of the radius is fixed to 1 arbitrary length units. (B) Intuition: the arms look straight for rational values and their number depends on the divergence angle. (C) However, slowly changing the divergence from an initial rational value (here 2/5) shows that arms can bend and even change in number.

called *opposite phyllotaxis.* Setting then $\alpha = 1/3$, yields three emerging straight arms. Likewise, for $\alpha = 1/4, \alpha = 1/5$, respectively 4 and 5 straight arms emerge as expected (Fig. 3.B). For $\alpha = 2/5$, the pattern seems to be identical to $\alpha = 1/5$. However, looking carefully, one can easily observe that the order in which the arms are visited is different (Schimper 1835). Let us identify the different straight arms for $\alpha = 1/5$ by their counter-clockwise azimuthal ordering, starting from the horizontal arm 1 to the right on Fig. 3.B. The arms are visited in the order $1, 2, 3, 4, 5$ for $\alpha = 1/5$ and $1, 3, 5, 2, 4$ for $\alpha = 2/5$. The numerator indicates the number of turns that are made before the organ initiation occurs again in the initial orientation (i.e. on arm 1). Equivalently, it also indicates the number of arms that are skipped from one initiation to the next initiation during the simulated growth process. $\alpha = 3/7$ then yields a motif with 7 straight arms that are all visited every 3 turns before the simulation comes back to the original azimuth for initiating an organ.

Shall we then conclude that if the divergence angle is defined by a fraction $p/q$ of a turn, then the motif always exhibits $q$ straight arms? Not quite so. Let us consider what occurs if one slightly changes the value of a divergence angle in the previous simulations. For example, instead of $\alpha = 2/5 = 0.40$, let us consider $\alpha = 0.401$. Note that this new divergence angle is also a rational as $0.401 = 401/1000$. Shall we expect a motif with 1000 straight arms ? When we run the simulation for this value of the divergence angle, we observe that this is not the case (Fig. 3.C). Instead, the previous 5 arms for $\alpha = 2/5$ are now slightly bending. If we increase the divergence angle, $\alpha = 0.405$, then $\alpha = 0.41$, the 5 arms can still be observed, but they bend even more. However, for $\alpha = 0.4286 = 2/7$, the 5 bending arms have disappeared and have now been replaced by 7 straight arms as previously observed. Then for $\alpha = 0.43 = 2/7$, the 7 arms bend again. However, both $0.41 = 41/100$ and $0.43 = 43/100$ are rationals. Why don't we see 100 straight arms instead respectively of the 5 and 7 observed arms?

**A different way to bend arms.** To solve this problem, let us consider a different way to bend the arms of our phyllotaxis motifs with our simple model. Instead of changing the divergence angle, let us keep it constant, say at $\alpha = 0.41$, as well as $V = 1 = R$, and change, between simulations, the time $T$ between the initiation of two organs, Fig. 4.A. For $T = 0.1$, we observe 5 spiraling arms, coiling counterclockwise away from the center. For a 2-fold decrease to $T = 0.05$, the bending of the 5 arms increases. Indeed decreasing $T$ progressively coils the arms tighter around the center: the angular positions of the points do not change, but their distance to the origin decreases. This also brings points in the different spirals closer together, so much so that the eye wants to connect newly neighboring points into new spirals. For $T = 0.05$, for instance, one can perceive, aside from the 5 original spirals, a new set of 17 spirals coiling clockwise from the origin. We say that the pattern is in a (5, 17) mode, or that its number of parastichies (the botanists' name for these spirals) are (5, 17), Fig. 4.B. At $T = 0.01$, in a figure reminiscent of a sunflower head, one can still perceive the 5 clockwise and 17 counterclockwise spirals close to the center, in much tighter coils than before. But on the outside, two more sets of spirals have emerged, one with 22 counterclockwise spirals, the other with 39 clockwise spirals. So the picture presents a transition of modes, something that commonly happens in asteracea's flower heads. Tracing the outer spirals from the outside in, one eventually hits a point where they cannot be naturally continued, as the spirals by 17 and 5 take over. Note that, the more spirals in one of these sets, the straighter the spirals: the 5-spirals are most coiled, the 39 are less so. For $T = 0.001$, all these spirals have coiled so much that the only pattern visible is that of 100 equally spaced straight arms shooting radially from the center. These are the 100 arms we long expected for our $\alpha = 41/100$!

It is important to note that, in these simulations, we have kept the parameters $R$ and $V$ constant, and varied only the plastochrone $T$ and divergence angle $\alpha$. We could have obtained the same result by keeping constant the plastochrone $T = 1$ arbitrary unit, and vary the speed

$V$ of primordia drift instead. What actually matters for the patterns is not each individual parameter but rather their product $VT$ that corresponds to the distance crossed by one primordium during one plastochrone. This defines a typical scale that must be compared with the size of the apex, *i.e.* the radius of the meristematic zone $R$. The patterning is thus governed by the ratio $G = VT/R$ between these two spatial quantities that characterizes the apex growth. This *growth index* can be measured directly from cuts or EM pictures, even without scale, from the respective distance of the organs (Richards 1951). From now on we will thus use more generally the two variables $\alpha, G$ (instead of $\alpha, T$), where $G$ can be varied by changing the value of either $T$, $V$ or $R$.

For a given divergence angle, the number of arms thus more generally depends on the growth index $G$, Fig4.A. As we have seen, decreasing $G$ increases the number of arms. But why do we eventually see 100 straight arms for $\alpha = \frac{41}{100}$ ? and how can we explain the numbers 5, 17, 22, 39 of spirals that we saw on our way to the 100?

**The numbers of spiral arms correspond to views of the divergence angle at different resolutions.** To understand this, let us consider with more attention the structure of our divergence angle $\alpha = 0.41$. We will make use of the fact that each real number can be increasingly well approximated by a unique series of fractional (rational) numbers called *its convergents*. For instance, $41/100$ can be increasingly well approximated by the sequence of rational numbers:

$$\left[ \frac{1}{2}, \frac{2}{5}, \frac{7}{17}, \frac{9}{22}, \frac{16}{39}, \frac{41}{100} \right]$$

Each fraction $p/q$ in this list is the best rational approximation of 0.41 that one can make with pieces of size $1/q$ or larger in a strong sense (see Box 2 and Supplementary information Section 2, as well as *e.g.* (Karpenkov 2013)). For example, $7/17$ is the strong best rational approximation that one can make of 0.41 with pieces of size $1/17$ or larger (i.e. it is a convergent of $41/100$).

So, how do these convergents appear in the geometry of our spirals? We have seen before that, for some range of growth index, when the divergence $\alpha$ is close to a rational $p/q$, the pattern displayed will have $q$ arms, and these arms become straighter as $\alpha$ moves closer to $p/q$. So seeing the successions of 5, 17, 22, 39 and finally 100 arms at different growth indexes is just the expression of the fact that $41/100$ is close to its convergents $\frac{1}{2}, \frac{2}{5}, \frac{7}{17}, \frac{9}{22}, \frac{16}{39}$. For different growth indexes, as the spirals coil onto themselves, those that were the least tightly wound, corresponding to the convergents with higher denominators, and whose points are farther apart, become progressively visible. This story generalizes for any real divergence angle[2] $\alpha$.

**When the divergence angle is the Golden angle, the number of visible spirals are consecutive numbers of the Fibonacci sequence.** In the previous sections, we considered exclusively rational divergence angle. However, all the previous conclusions remain valid for irrational numbers. Indeed, for irrational numbers as well, a unique list of convergents can be defined that give a multiresolution approximation of this number (see Supplementary information Section 2).

What about the Golden angle? In the 1830, a pair of young German scientists, Schimper and Braun (Schimper 1835, Braun 1831) made the first observations of Fibonacci phyllotaxis. They defined the divergence angle and hypothesized, given their observations that most often, it must belong to the sequence of *rationals*

$$\frac{1}{2}, \frac{1}{3}, \frac{2}{5}, \frac{3}{8}, \cdots$$

---

[2]Note that strictly speaking, for a general $\alpha$, it is guaranteed that at least one of the two mode numbers is the denominator of a convergent. One can show that the second mode number is either also the denominator of another convergent ($\approx 40\%$ of the cases), or the denominator of a best approximation close to the first convergent.
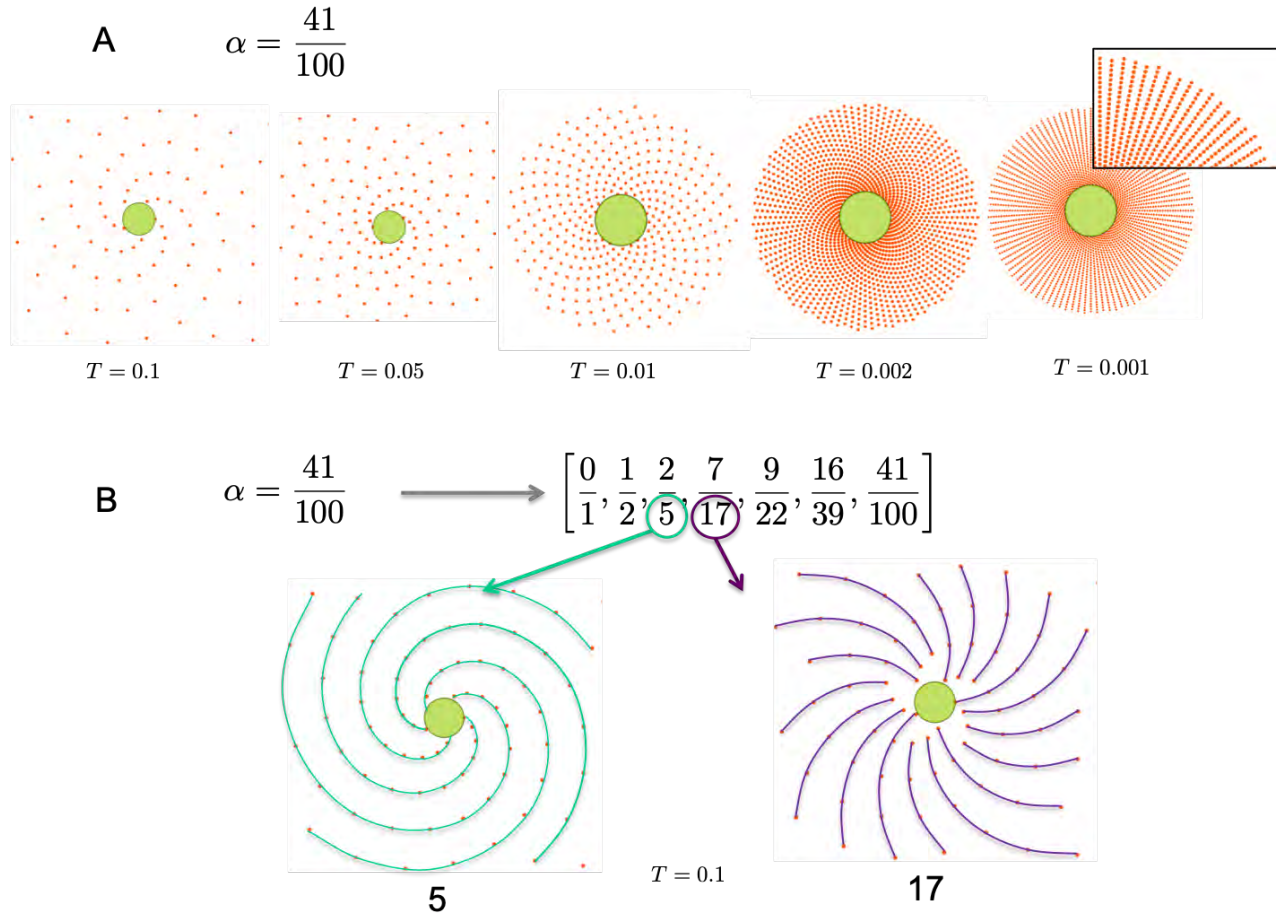
Figure 4: **Browsing convergents: exploring the structure of a number through scales**. (A) Decreasing the value of the plastochrone while keeping the divergence angle constant, here $\alpha = 41/100$, also induces bending of spiral arms. After some point, the spirals merge and a new set of arms appears – here 5 original bending arms (left) are progressively replaced by 100 straight arms (right, close-up). (B) For each pattern (here for $T = 0.1$), one can observe the spiraling arms in two families of parastichies, turning in opposite directions, as in plants, and whose number are often consecutive denominators in the list of convergents of the divergence angle, here $\frac{1}{2}, \frac{2}{5}, \frac{7}{17}, \frac{9}{22}, \frac{16}{39}, \frac{41}{100}$. The number of spirals in these two families define the mode. Here the mode is $(5, 17)$. In A, the modes are successively $(5, 17), (22, 17), (22, 39)$ until we reach the 100 straight arms configuration, where the other 39 spirals are less visible.

quotients of numbers that are two apart in the Fibonacci sequence. Independently, the equally young French brothers Bravais (Bravais & Bravais 1837) made the same kind of observations, except that they always saw, in their hundreds of observations, bending arms (or, on a stem, skewed vertical rows of organs). They computed the continued fractions of the quotients above, and noticed that they were all truncations - that is, the convergents - of the same *infinite* continued fraction:

$$\cfrac{1}{2 + \cfrac{1}{1 + \cfrac{1}{1 + \cfrac{1}{1 + \cfrac{1}{\ldots}}}}}$$

the limit of which "Algebra teaches to compute", as they say, is:

$$\frac{3 - \sqrt{5}}{2},$$

which we recognize as $\gamma = \frac{1}{\phi^2}$ (see Box 1). Thus was born what we now call the golden angle! Note that while the Bravais note that $\gamma$ is irrational - explaining the bending of arms - they make no mention of its relation to the golden ratio, whose relation to the Fibonacci numbers was not as widely known as today, see Box 1 and Supplementary Information Section 3 for more on the relationship between $\phi$ and $\gamma = 1/\phi^2$ and their convergents.

According to what we discussed above, the number of spirals that are observed in motifs corresponding to an angle of divergence $\gamma$ are consecutive denominators of its sequence of convergents, that is the fractions $\frac{1}{2}, \frac{1}{3}, \frac{2}{5}, \frac{3}{8}, \frac{5}{13} \ldots$ whose limit is $\gamma$. That is to say, the number of parastichies must be pairs of consecutive Fibonacci numbers. See Fig. 5.A. [3]

So is that it then? Must all plants with Fibonacci phyllotaxis have constant divergence angle $\gamma$? This is the hypothesis that the Bravais made. After all, here was one number that could explain the vast majority of the many plant patterns they observed, and whose divergence angle they measured (by taking averages over several turns) to be very close to $\gamma$. This hypothesis has stuck to many as a diktat for close to 200 years. Yet, wise beyond their years, the Bravais ((Bravais & Bravais 1837), p.73) warn us that this might only be a guiding hypothesis (our translation):

*"Let us note once more that we are not pretending to prove in a rigorous manner that the divergence angle is constant, but we deem it as the most likely hypothesis in our present state of knowledge; were it only a theoretical idea to verify, it would still be a useful guide in the study of plant symmetry, or Phyllotaxis, as Mr. Schimper calls it."*

**Summary.** Altogether, this section shows that, via a simple regular spiral model, there is a strong but subtle mathematical link between divergence angles and parastichies. In short, spiral patterns are simply geometric representations of the fixed divergence angle with varying precision levels that are determined by the growth index. Straight arms indicate that the organs move sufficiently slowly away from the center so that their positions provides an exact estimation of the divergence angle. In contrast, bending arms (spirals) reveal that the growth index is too coarse to represent exactly the divergence angle. Depending on divergence angle and growth index values, either one or two families of spirals can be observed (e.g. Fig. 4). Reciprocally,

---

[3]We will see that, since $\gamma = 1/\phi^2$ its convergents are also easily derived from the sequence of convergents of $\phi$, $\frac{0}{1}, \frac{1}{2}, \frac{1}{3}, \frac{2}{5}, \frac{3}{8}, \frac{5}{13}, \frac{8}{21}, \frac{13}{34} \ldots$, which are quotients of successive Fibonacci numbers, see Supplementary Information Section 3)
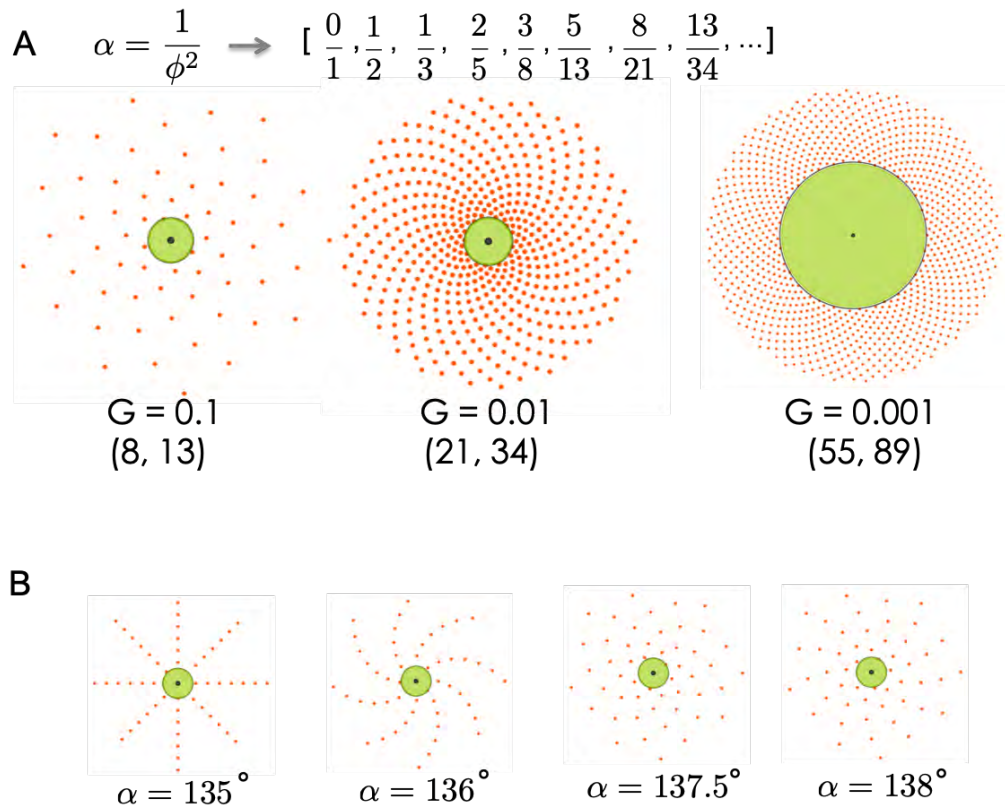
Figure 5: **Divergence angle corresponding to the Golden angle**. (A) Variation of the spiral pattern for decreasing growth index $G$ for a divergence angle = golden angle (B) Drastic change of spiral patterns in the neighborhood of the golden angle (the growth index is fixed to $G = 0.1$).

the numbers of clockwise and anti-clockwise spirals inform us on the possible underlying (non-observed) divergence angle (assumed to be constant in this idealized situation). This result is sometimes referred to as the fundamental theorem of phyllotaxis (after Adler in the 1970s and Jean in the 1980s in particular, who generalized somewhat what the relation that the Bravais discovered) (see Box 4).

The above geometric model assumes that i) growth index, and divergence angle are independent variables and ii) divergence angle and growth index have constant values. If the divergence angle is set to the golden angle, classical families of Fibonacci spirals become visible. However, many other phyllotaxis modes, different from the Fibonacci ones, can be observed for other values of the divergence angle, whether it be in nature (where they are rare) or in simulations.

The fact that Fibonacci modes are so largely predominant in plants with spiral phyllotaxis thus suggests that something else is probably constraining the system to keep it in this Fibonacci regime. In principle, either the divergence angle or the parastichies could actually be constrained by the growth processes to take precise values, consequently restricting the range of values taken by the other through the above geometrical link. However, both cases raise interpretation difficulties: If developmental constraints act directly on spirals, selecting specific numbers of arms, how can these numbers be consecutive numbers of the Fibonacci sequence ? On the other hand, if developmental constraints directly regulate the value of the divergence angles, how can one explain that this value is most of the time close enough to the golden angle ? Even for divergence angles deviating only little from the golden angle (e.g. $\alpha = 136, 137, 138, \ldots$), we observed spiral patterns showing large gaps between spiral arms (parastichies) and modes that are not observed in plants (Fig. 5.B), e.g. (Prusinkiewicz & Lindenmayer 1990). If the divergence angle were indeed constant and equal to the golden angle, how could the plant maintain a precision such that only Fibonacci spirals are observed at a macroscopic level? And why could other divergence angles be seen some of the time, while often showing parastichy numbers related to the Fibonacci type of sequence (Lucas, Bijugate) in those cases?

The solution to these paradoxes lies partly in the fact that the divergence angle and the growth index are not independent variables in real plants.

# 4    The coupling between growth index and divergence angle in plants

**Taking into account organ primordia contacts.**   In the previous simple geometric model, we were interested in the positions of primordia without considering their actual size nor their physical or chemical interaction. However, in meristems, young primordia may encompass a tissue region of several cells of diameter and inhibit the initiation of other organs in their immediate neighborhood. As a whole, each primordium defines a zone of exclusion around it, where no other organ can form. The exact origin of the underlying bio-physical mechanism seems to be mainly of molecular nature (Reinhardt et al. 2003, Barbier de Reuille et al. 2006, Besnard et al. 2014), although a physical (mechanical) contribution cannot be excluded (Galvan-Ampudia et al. 2016). In the sequel, we identify the primordium region and the inhibition zone around it as the "primordium" as a whole, without paying attention to distinction between the primordium proper and its lateral inhibition nor to the exact nature of the inhibition, which are not essential to this discussion.

**Toward a more mechanistic model.**   Mechanistic models taking into account such inhibitory action between organs at the meristem abound. The most common view is that primordia are initiated at the rim of the central zone (CZ) that is crowded by young primordia (Figs. 1.A-left, 2.A, 7.A). By their local inhibitory action, these primordia altogether inhibit

the formation of new primordia as long as they keep close enough to the CZ. However, due to growth, the CZ drifts away from the existing primordia and new primordia can form as soon as sufficient space is available at the CZ rim. This process results in contacts between primordia at the edge of their individual inhibitory zones (Hofmeister 1868). With growth, this pattern of contacts is often preserved in compact structures (Fig. 7.B) and is still visible in elongated stems with the vasculature (Plantefol 1948). Altogether, the classical hypotheses governing local interactions between organs at the tip of growing meristems can be summarized as follows:

i. *Circular symmetry*: The meristem can be approximated by a surface of revolution (disk, cone, cylinder...);

ii. *Center inhibition*: no organ can form in the central zone of the circularly symmetric meristem;

iii. *Primordia inhibition*: young primordia inhibit the formation of new organs around them;

iv. *Tissue growth*: due to the tissue growth, previously formed primordia are left behind the growing tip, or equivalently they are seen moving radially away from the initiation zone at the tip of the SAM. The primordia themselves grow in size keeping their original contacts;

v. *Deterministic initiation*: primordia form at the edge of the CZ *when* and *where* overall inhibition is sufficiently low, thus establishing initial contacts with the closest primordia.

Many of the models of phyllotaxis morphogenesis imply, more or less explicitly, these five major assumptions ((Schwendener 1878, Snow & Snow 1952, Veen 1973, Adler 1974, Mitchison 1977, Douady & Couder 1996a,b, Atela et al. 2003, Smith & Prusinkiewicz 2006, Pennybacker et al. 2015) among others.). In the simplest (and oldest) instance of these models (Schwendener 1878), the geometry of meristems (Fig. 6.A) is abstracted as a packing of circular organs, for which parastichies can be identified by joining each primordium to the two preceding ones in contact with it (Fig. 6.C). Such parastichies are sometimes called *contact* parastichies for this reason. Depending on whether one concentrates on the top, so-called "centric" view of the meristem (Fig. 6.A & C) or on a side "cylindrical" view (Fig. 6B & D) the underlining geometry is either approximated by a planar annulus or a cylinder. It turns out that these views can be put into a one-to-one mathematical correspondence (see Supplementary Information Section 1). In fact Figure 6.C was obtained from 6.D using that very correspondence. For now, it suffices to say that, given this correspondence, the geometric assumptions that follow are not overly simplistic.

We thus represent the region around the meristem of diameter $D$ by a cylinder which, unrolled, turns into a rectangle of width $C = \pi D$, the circumference of the CZ. The upper boundary corresponds to the rim of the CZ and the primordia are represented as disks with identical (for now) diameter $d$ on the surface of the cylinder (Fig. 7D). As the geometry of this system is preserved for identical ratios $d/D$ up to a scaling factor, we conveniently set the CZ diameter $D$ to 1 in our model, meaning that $d$ should be thought of as the ratio of the primordium diameter over the diameter of the CZ. In this cylindrical representation, angles between two primordia are represented by the horizontal distance between their centers and are comprised between 0 and 1: as before, we choose the unit of angle to be a turn. Likewise, assuming as before that the displacement velocity $V$ is 1, the vertical distances between primordia centers, corresponding as before to the growth index $G$, can be thought also as the time lag that separates their initiation. Divergence angles $\alpha$ are thus represented by the horizontal component of the vector between pairs of consecutively initiated primordia, while growth indices $G$ correspond to their vertical components.

Using this cylindrical representation, we can now go beyond descriptive models and propose a mechanism of pattern formation. In this cylindrical setting, our five preceding rules come
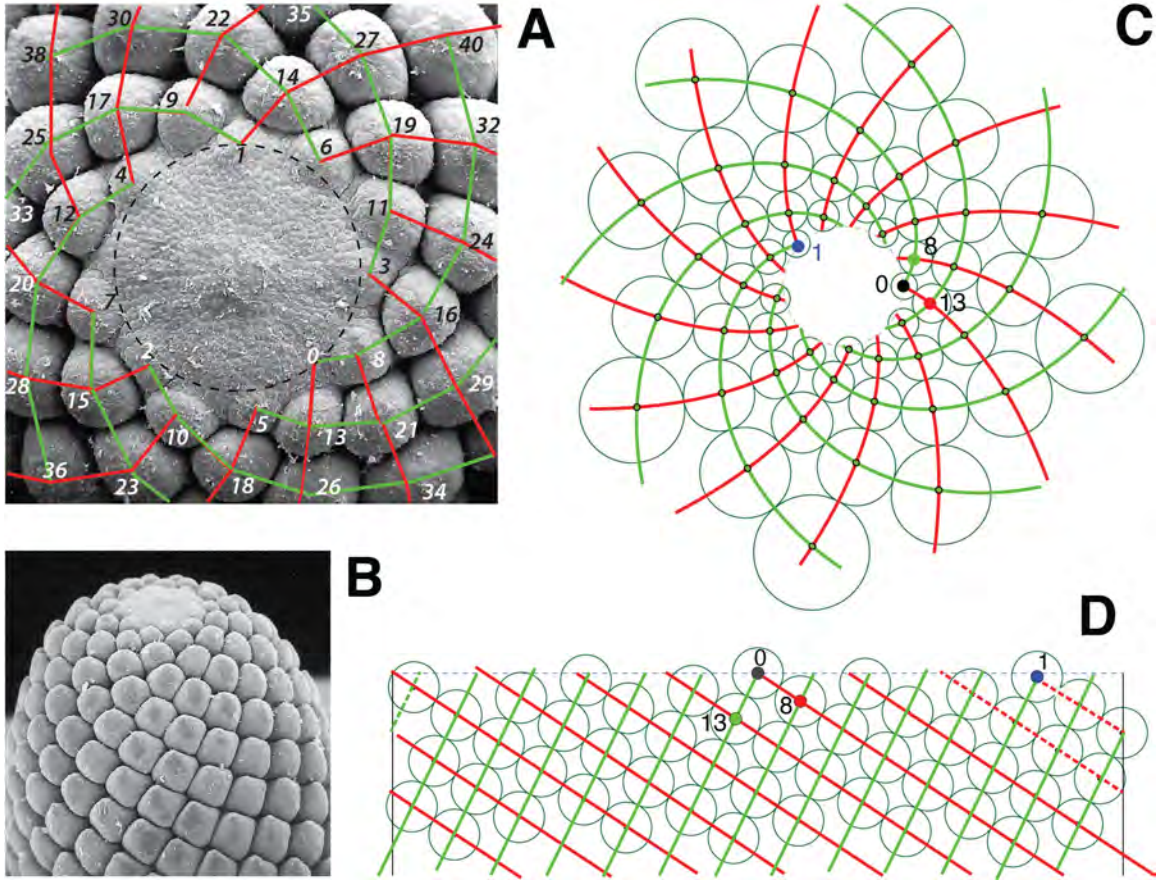
Figure 6: **Spiral and cylinder lattices.** (A) Top (centric) view of a picea meristem (micrograph courtesy of Rolf Rutishauser). The primordia shown here were to form pine needles. There are 8 green contact parastichies and 13 red ones. The divergence angle is not far from the Golden angle. (B) A sideview of the same meristem (micrograph courtesy of Rolf Rutishauser) showing the different geometries of the same configuration. (C) Logarithm spiral lattice structure with (8, 13) phyllotaxis mimicking the picea in (A). The (almost circular) virtual primordia are expending away from the CZ at a speed proportional to their distance from the center. (D) Cylindrical lattice of mode (8, 13) mimicking the unrolled, side-view of the pattern. Primordia are modeled as disks arranged in straight, criss-crossing parastichies joining disks in contact. The figures in C and D are related in a very specific mathematical sense here, see Supplementary Information Section 1. Note that there is no contact between the organs in their order of apparition (along the generative spiral), as 0, 1 and 2 are far apart, but there are contact with the one forming the contact parastichies, here 0 is in contact with 8 and 13.

down to a very simple rule (initially introduced in (Schwendener 1878), ten years after its description by Hofmeister).

**Disk stacking model:** *Stack disks one by one in the lowest possible place on the previous disks without overlap, on the surface of a cylinder of circumference 1*

As a consequence of the model's assumptions, each primordium (represented as a disk) is tangent to *two* (or more rarely three) "parent" primordia below. By construction, its parents are its closest older neighbors. Contrary to the initial simple geometric model in Section 3, this model enforces contact between every new primordium and at least two previous ones. This contact constraint drastically reduces the space of possible observable pairs $(\alpha, G)$ as we will see.

**Coupling of growth index and divergence: the van Iterson diagram.** Assume for now that the pattern generated by this mechanism has constant $\alpha$ and $G$ between each initiation. Joining nearest neighbors in such a pattern gives rise to two sets of straight parallel lines, the parastichies, which crisscross the rectangle into a *lattice motif*, reminiscent of the wooden lattice structures, used to support climbing plants along walls. For that reason, these regular disk patterns are called *cylindrical lattices*, or lattices for short (see an example in Figure 6D). Note that, rolled back on the cylinder, these straight parastichies become helices.

The number of parastichies in each family (also called the mode of the lattice as for the previous spiral model) can be nicely read off the index of the two disks closest to the reference Disk 0 (Braun 1831): if the closest disks are Disks 8 and 13 for instance, as in Figure 6D, there must be 8 parastichies parallel to the one through Disks 0 and 8 (red in the figure)- namely the ones through Disks 1 and 9, through Disks 2 and 10, on up to the one through Disks 7 and 15. Likewise there are 13 parastichies parallel to the (green) one through Disks 0 and 13. So the parastichy numbers are (8, 13) here. They are also easily counted in the corresponding centric view (Figure 6C).

Not all lattices can be obtained by the stacking process. For instance, the lattice of Figure 7A cannot be the result of stacking: Disk 0 would have to be tangent to its closest neighbor, 2 and 3. For this double tangency to happen, since all the disks have same diameter $d$, the centers of Disks 2 and 3 should be equidistant to 0, which they're not in this case. In contrast, the lattice of Figure 7B is compatible with our contact model: Disk 0 rests tangentially on Disks 3 and 5. This means that the tiling created by the crisscrossing of the parastichies is made of *rhombic tiles*, with 4 equal sides, and this type of lattice is called a *rhombic lattice*.

In general, each value of $(\alpha, G)$ thus gives rise to a lattice, rhombic or not, with disk diameter $d$ that is equal to the distance between Disk 0 and the disk closest to it. This pair $(\alpha, G)$ thus corresponds to a specific mode $(i, j)$ (indices of the closest neighbors of a reference Disk 0) characterizing its lattice geometry. If we color, using a computer program, the points of the plane $(\alpha, G)$ that bear identical mode $(i, j)$, we obtain regions depicted on Fig. 7. Each region is a "quadrilateral" deformed into an asymmetric kite bounded by four arcs of circles, where each of these circles is centered on the $\alpha$ axis.

Requiring that the lattice be rhombic imposes a subtle relationship between $\alpha$ and $G$. In 1907, van Iterson (Van Iterson 1907), inspired by the work of Schwendener (Schwendener 1878) described the set of all possible pairs $(\alpha, G)$ that would generate rhombic lattices, where contact is maintained between parastichies of the disk-like organs. This set, now called the van Iterson diagram, forms in the $(\alpha, G)$ plane a characteristic upside down tree, whose branches are made of arcs of semi-circles centered on the $\alpha$ axis and shown in black on Fig. 7, with infinitely many branching points (see also Box 5). Each branch of the van Iterson diagram constitutes a "diagonal" of one of the previous quadrilaterals, joining 2 opposite vertices. Hence every lattices
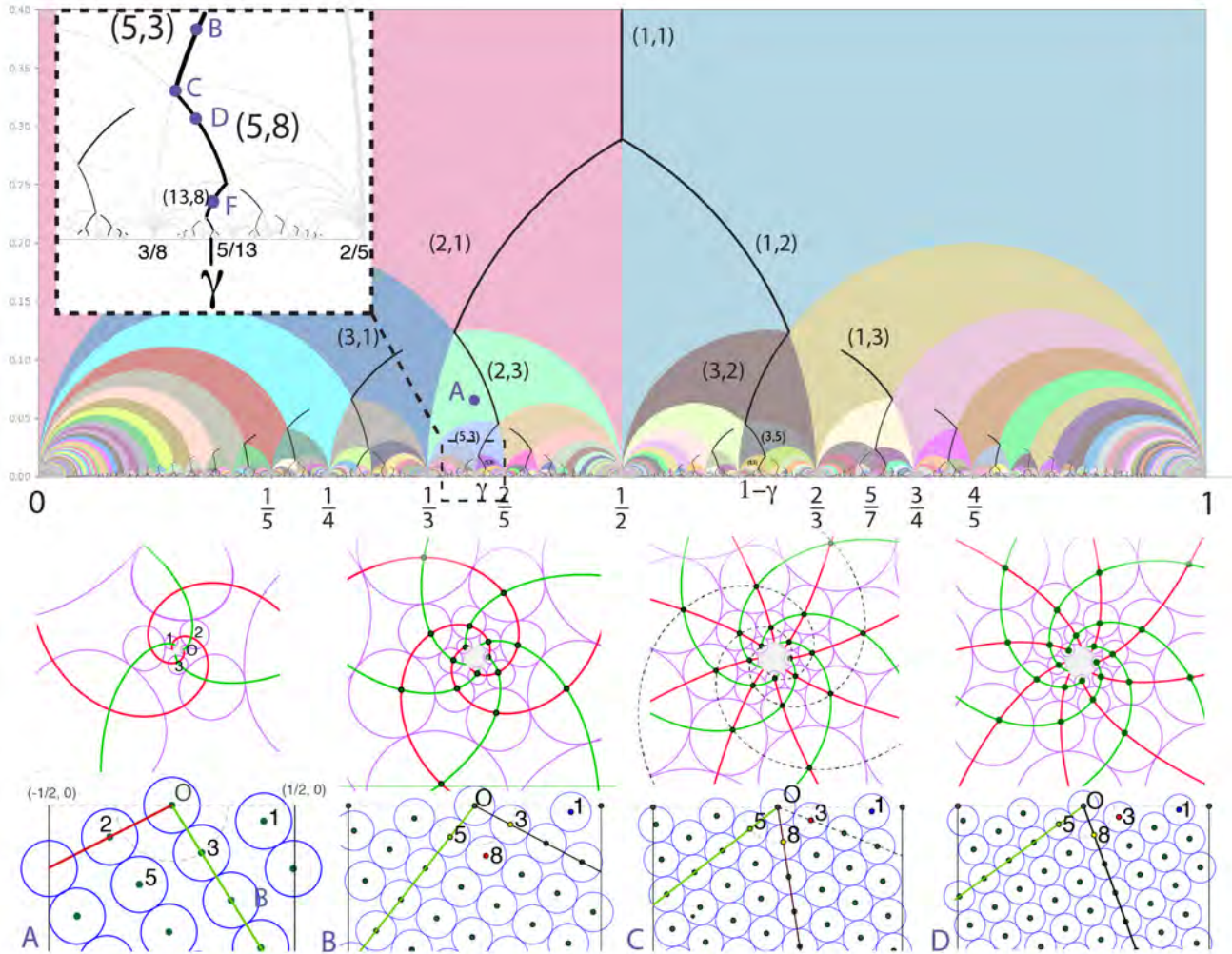
Figure 7: **The $(\alpha, G)$ plane with the regions of constant mode and the van Iterson diagram.** The top picture is the $(\alpha, G)$ plane, where each point corresponds to one lattice with a close up (dashed square). The colored "quadrilaterals" represent regions where all corresponding lattices have the same mode, or parastichy numbers. The figures A, B, C, D show the lattices whose values of $(\alpha, G)$ is marked by points of the same name above. Point F corresponds to the lattice of Figure 6. Each lattice is topped by the spiral configuration that corresponds to it, in centric view. B, C, D (and F) are all rhombic: the two closest points to 0 are in each case equidistant to it. Accordingly the points B, C, D and F are all on the van Iterson diagram, drawn in black. As one travels down the main branch of the van Iterson diagram, starting in Region (1,1) and making a left at (2,1), one crosses the different region with successive Fibonacci numbers, with the divergence $\alpha$ oscillating between the convergents $\{1/2, 1/3, 2/5, 3/8 \ldots\}$ of $\gamma$. At the branching point C, there are 3 disks tangent to Disk 0, and accordingly 3 sets of parastichies. Decreasing $G$, the only choice compatible with the stacking model is the mode $(5, 8)$: Disks 8, and 3 are on the same side of 0, and can't be its parents. Making a right on the the branch $(1, 2)$ instead would yield the same Fibonacci pattern but with opposite chirality.

16

on a branch have the same parastichy numbers (or mode). At a vertex, 3 quadrilateral regions meet. This is because the vertex corresponds to a lattice with three sets of contact parastichies: each disk has 3 parents in this case.

Below these transition points, there are two arcs of circle corresponding to two new possible modes, choosing one pair or the other among the three possible contacts. However, one possibility does not correspond to a growing pattern, as the two parastichies, or parents, would wind in the same direction, which is not possible (Fig. 7 C). Accordingly, in Figure 7 the parts of the arc of circles these lattices correspond to were removed from the original van Iterson tree. This "pruning" of the van Iterson tree isolates two branches of the diagram stemming from mode (1, 1) and $\alpha = 1/2$, and through modes (2, 1) or (1,2), to increasing Fibonacci modes and $\alpha$ tending to $\gamma$ or $1 - \gamma$.

The pattern being rhombic can be seen as some kind of compactness condition for a lattice which reproduces what is usually seen in plants: parallel parastichies in a family are not separated, but rather their primordia are tangent. And the same holds for the contact spiral parastichies in the corresponding centric view. For example, to better mimic the picea of Figure 6A and B, the lattice we chose in 6D is a rhombic lattice, of parastichy numbers (or mode) (8, 13). On the other hand, the lattice of Figure 7A, with its isolated parastichies, is not what a nascent plant pattern looks like.

**Does this explain canalization toward Fibonacci phyllotaxis?** In front of this remarkable mathematical structure that seems to encapsulate the universe of all possible regular phyllotactic structures, one is tempted to conclude that the singling out of the Fibonacci paths of the van Iterson diagram *is* the explanation of the canalization of plants toward Fibonacci phyllotaxis. Indeed, in the embryo of a dicotyledon, the two first leaves are opposed and the initial divergence angle is $180° = 1/2$ turn. This corresponds to (1,1) phyllotaxis. During plant growth, the meristem scales up in size, presumably together with its central zone while primordia essentially are initiated with the same size and keep the same growing rate. This results in a progressive decrease of the ratio parameter $G = d/D$ between primordia diameter and stem diameter. Due to the contact constraint, the divergence angle and the growth index of the pattern evolves accordingly to stay along the main branch of the Van Iterson tree, inevitably leading to Fibonacci phyllotaxis, with the divergence tending to $\gamma$ (Douady & Couder 1992, Atela et al. 2003).

But, what do we really mean by "the pattern evolves"? The van Iterson diagram corresponds to perfectly regular figures, the rhombic lattices, where each primordium has the same diameter $d$, and everything looks the same from any point of the pattern (Fig. 6 and 7). When the pattern changes with decreasing $G$ however, we must accommodate the ideal of rhombic lattices to the fact that the disks do not all have same diameter $d$, and that the pattern has potentially different parastichy number pairs at different spatial positions. At any rate, it certainly is not a rhombic lattice any more. One way out of that quandary is to argue by approximations: assuming that $d$, and therefore $G = d/D$, varies sufficiently slowly, and in stages, the pattern would stabilize to successive *portions* of rhombic lattices. This is essentially the approach explicitly or implicitly taken in (Douady & Couder 1996b, Atela et al. 2003), the first numerically, the second analytically.

Unresolved issues remain however: the numerical experiments in these papers show that the patterns may not always converge to rhombic lattices (although, for the model it studies, not one of disk stacking, (Atela et al. 2003) does show that steady states rhombic lattices are *locally* attracting). Indeed, sometimes the stabilized pattern, although still lattice-like, exhibits seemingly erratic divergence angles corresponding to permutations in the primordia order (Douady & Couder 1992, 1996b, Atela & Golé 2007). While a similar phenomenon has also been observed in plants (Couder 1998, Besnard et al. 2014, Refahi et al. 2016), whether it

takes its origin in such an erratic convergence is still unclear. Moreover, the time necessary for a reasonable convergence may well be beyond the number of generations of organs produced by plants. And what *does* happen during the transitions between these periods of stabilization anyway? How fast can $G$ decrease? How can one account for the inevitable noise occurring in the process? Not to mention that, for the disk stacking process, rhombic lattices are actually *not* attracting: A perturbation of a rhombic lattice, will usually not converge back to the original (Atela & Golé 2007, Golé & Douady 2019). Are all these models irremediably inadequate then, or are we asking them to answer misconceived questions?

To reduce the gap between these theoretical aspects of phyllotaxis and observations, we need to focus on a more local level, somewhere between the individual primordia and the whole pattern, on the part of the configuration that is more immediately in charge of its evolution. In the process, we might loose, at least temporarily, the elegance of the viewpoint of a plant pattern as represented by just one pair of parameters $(\alpha, G)$ and the underlining mathematical beauty of the mode landscape and its associated van Iterson tree. But the hope is to gain flexibility to actually understand pattern transitions, and canalization in a less idealized fashion. One may note that even if we stick to our ideal of a plant structure as a regular lattice with constant $(\alpha, G)$ exhibiting Fibonacci phyllotaxis, our discussion has shown that its divergence $\alpha$ need not be exactly the Golden Angle $\gamma$, although it will be comprised between its convergents. So the myth, initiated by the Bravais (Bravais & Bravais 1837) of the divergence being equal to $\gamma$ is already shattered! Or has it been enriched?

# 5    Canalization of Fibonacci phyllotaxis via fronts

As suggested in the previous section, we need to concentrate on the portion of a phyllotactic pattern that is most immediately responsible for the future of the pattern. In plants it would be the most recent layer of primordia, directly encircling the meristem. In the disk stacking model, this corresponds to the top layer of disks encircling the cylinder. We call this layer a (primordia) *front* (Hotton et al. 2006, Golé et al. 2016). To capture the idea that a front represents a snapshot of the latest primordia at a given time, we require that the next disk added to the structure be tangent to disks of the front, and higher than any disk in the front. The history of a pattern can be traced via its successive fronts.

Fronts can be represented by a zigzagging curve joining centers of adjacent primordia in the front, see Fig. 8. The front parastichy numbers are the numbers of line segments joining adjacent primordia of the front, going up or down as we move along the front (red and green in our figure). In regular patterns (such as lattices), these front parastichy numbers correspond to the numbers of parastichies of the whole pattern.

Even if the disks remain of constant size, the evolution of the pattern can be surprisingly subtle (Golé & Douady 2019). But the true power of the model arises as one changes the size of the disks with respect to that of the cylinder, that is, if we change the parameter $G = d/D$. This change of parameter occurs when the meristem's diameter $D$ grows as the stem matures, while the primordia' diameters remain of roughly equal size $d$. In our simulation we left $D$ constant and decreased $d$ instead, which has the same overall effect. See (Atela 2011) for simulations with increasing $D$.

Let us start with a front that is regular enough, i.e. with similar up and similar down segments and stack disks on it, in the lowest possible place without overlap, while slowly decreasing the size $d$ of the disks as they move up. The evolution of the front automatically generates a recursive "Fibonacci machine", where a front with parastichy numbers $(i, j)$ with, say, $i < j$ eventually begets another with parastichy numbers $(i+j, j)$, see Fig. 8.C and D. When starting with $i = 1, j = 1$ - which monocotyledon plants do, with the cotyledon serving as initial leaf -
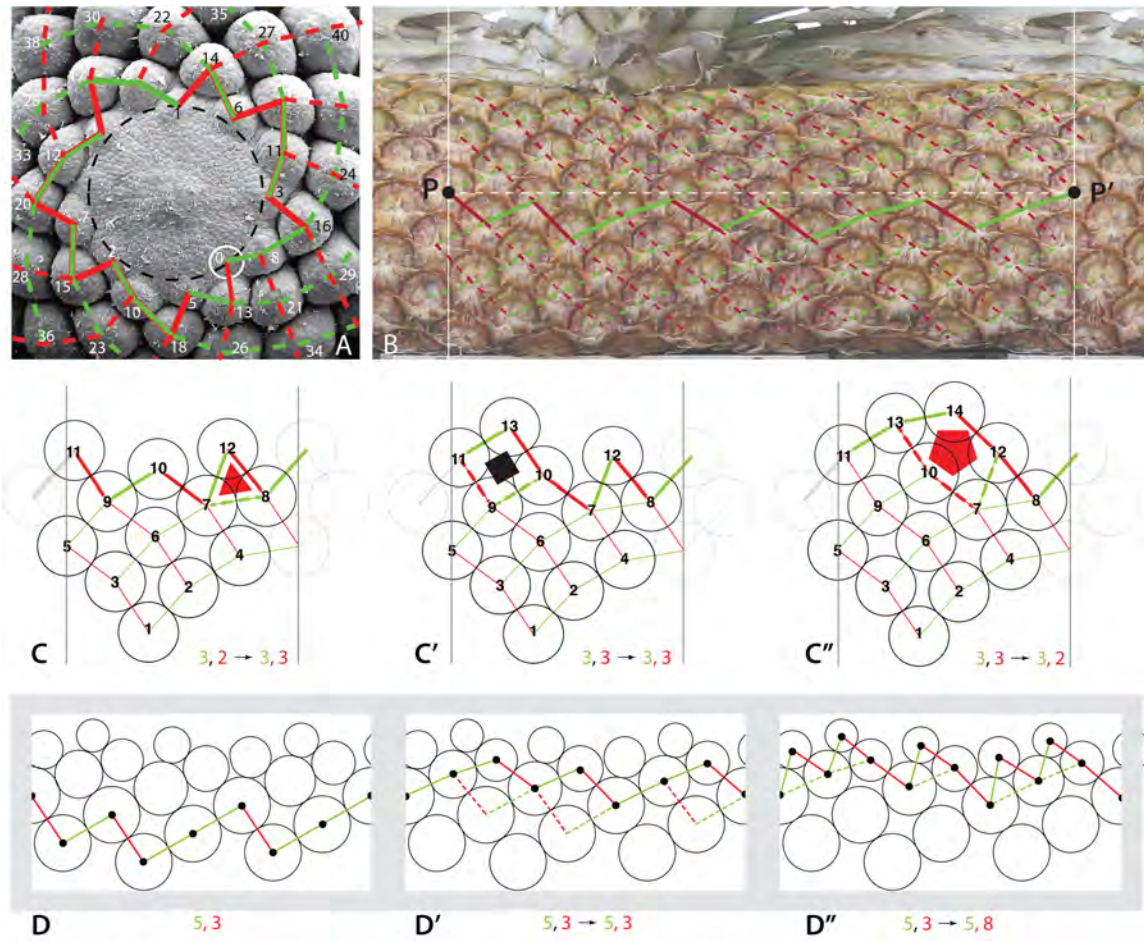
Figure 8: **Fronts as Fibonacci machines.** (A) The picea meristem of Fig. 6 with its latest front underlined in solid red and green. The front determines the placement of the next primordium, numbered 0 here. One can count 13 green segments and 8 red ones joining adjacent primordia in the front, which correspond to the number of spiral parastichies (B) Digitally rolled out pineapple. The white vertical lines represent the same vertical line on the pineapple, and points $P$ and $P'$ are also identical on the pineapple. The pattern is 5, 8 here, as shown by the counting the segments in the front joining $P$ and $P'$, or by counting the green and red (dashed) parastichies. (C) A Triangle transition increases the parastichy number by one. (C') a quadrilateral transition keeps the parastichy numbers unchanged. (C") A pentagon transition decreases a parastichy number by 1. (D-D") Fibonacci transition from 5, 3 to 5, 8: the starting front in (D) has 5 up, 3 down segments. The up segments are roughly parallel, as are the down segments. (D') At first the transitions are all quadrilateral. But as the disks decrease in size, and the front angles open up, it forces triangle transitions (D"). These occur on the flatter segments (the green, up segments here, as there are more of them). Each triangle adds an extra (red) down segment, for a total of 5 new down segments, which added to the 3 old ones gives 8 of them. On the other hand, there are no extra up segments, but the existing ones have become more slanted again, with roughly equal angles, setting the stage for the next round.

19

this recursive mechanism yields the Fibonacci sequence[4]. To check the prevalence of the scenario systematic simulations that sweep the parameter plane of possible angle of (1, 1) fronts and rates of decrease of $d$, consistently detect Fibonacci pattern formation when the angle of the original front is not too large, and $d$ (or $G$) decreases slowly enough, see (Golé et al. 2016, Figure 15)[5].

As some plants reach inflorescence, the parameter $G$ may revert to increasing instead, as the meristem ceases to grow and primordia fill it in, see (Douady & Couder 1996b, Douady & Golé 2017, Figures 2 and 3). In this case pentagon transitions provoke a decrease in parastichy numbers, often along the Fibonacci sequence as well. Regular patterns in this latter phase are better represented by the Archemedian spirals of our first model from Section 3 (Fig. 9.C).

**The golden angle as an emergent phenomenon.** The fact that we did not have to invoke the angle of divergence in the front-based explanation of Fibonacci pattern formation in Fig. 8 should make it clear that it is not the driving concept behind phyllotaxis morphogenesis. Is it a by-product then? Even this appears in doubt when looking at the graph of the divergence angle along simulated Fibonacci growth Fig. 10.B. Indeed the divergence angle oscillates closer and closer to the golden angle at first. But then it breaks up in large oscillations, even though the pattern itself (Fig. 9B) seems relatively regular. A closer inspection reveals that the angles between which the divergence oscillates are all close to *multiples* of the golden angle (Douady & Couder 1996b, Golé et al. 2016). And the explanation becomes clearer when one inspects the order in which the disks appear on the front: as the disks become smaller, small irregularities of the front may induce permutations in the stacking order of these new disks on the front (Fig. 11.A and E). This permutation phenomenon is not only an artifact of the simulation: it has been observed in arabidopsis and Birch catkins (Besnard et al. 2014, Douady & Golé 2017) and studied in the framework of stochastic (random) processes (Refahi et al. 2016).

So, do these wide fluctuations of the divergence angle entirely invalidate the hypothesis of the golden angle being central to phyllotaxis? Not quite yet... Interestingly, taking the mean of the divergence angle over each front, even in this disordered case, restores the regularity of the divergence angle, which then closely follows the oscillating convergence to the golden angle, along the van Iterson tree branches, seen in patterns with slowly decreasing $G$ (Fig. 10.D). In this precise sense then, while it is not its mechanistic principle, the golden angle divergence *is* an emergent byproduct of Fibonacci patterning. The geometry of fronts, with its finite number of combinations of up and down segments offer some privileged slots for the next disks to be stacked. These slots remain essentially the same under perturbation, and while the order in which they are filled may vary, causing the wide variations in the divergence angle, these variations are averaged out to a value close to the unperturbed lattice case. Interestingly, the Bravais brothers (Bravais & Bravais 1837) who, as we have seen, cautiously heralded the golden angle as the organizing principle of Fibonacci phyllotaxis, detail their data gathering method for the calculation of the divergence angles of many specimens: for a plant with an $(i, j)$ phyllotaxis, it consists of averaging the divergence over $i + j$ consecutive nodes, *i.e.* s many nodes as there are in a front!

If the mean oscillates closer and closer toward the golden angle, it is worth noting that in the fronts simulations, there is always some irregularity, and each transition induces additional irregularity (the triangle bifurcations cannot all happen at the same level and at the same time).

---

[4]In dicotyledons, a break of symmetry, where the pattern transitions from (2,2) to (2,3) is frequent, and also leads to subsequent Fibonacci front parastichy numbers (Couder 1998). Note that we assumed nothing about $\alpha$ being constant, or near the golden angle here. Alternatively, the pattern evolves into bijugate modes, with parastichy numbers that are $(2i, 2j)$, where $i, j$ are successive Fibonacci numbers, or to $(1, 3)$ and subsequent Lucas numbers. These two are next most frequently recorded non Fibonacci patterns

[5]The simulations show a region of consistent Fibonacci transitions such as depicted in Figures 9 and 11 for a rectangle in the parameter region with $.58 < d < .5$ and the rate of decrease of $d$ vs. height less than .1.
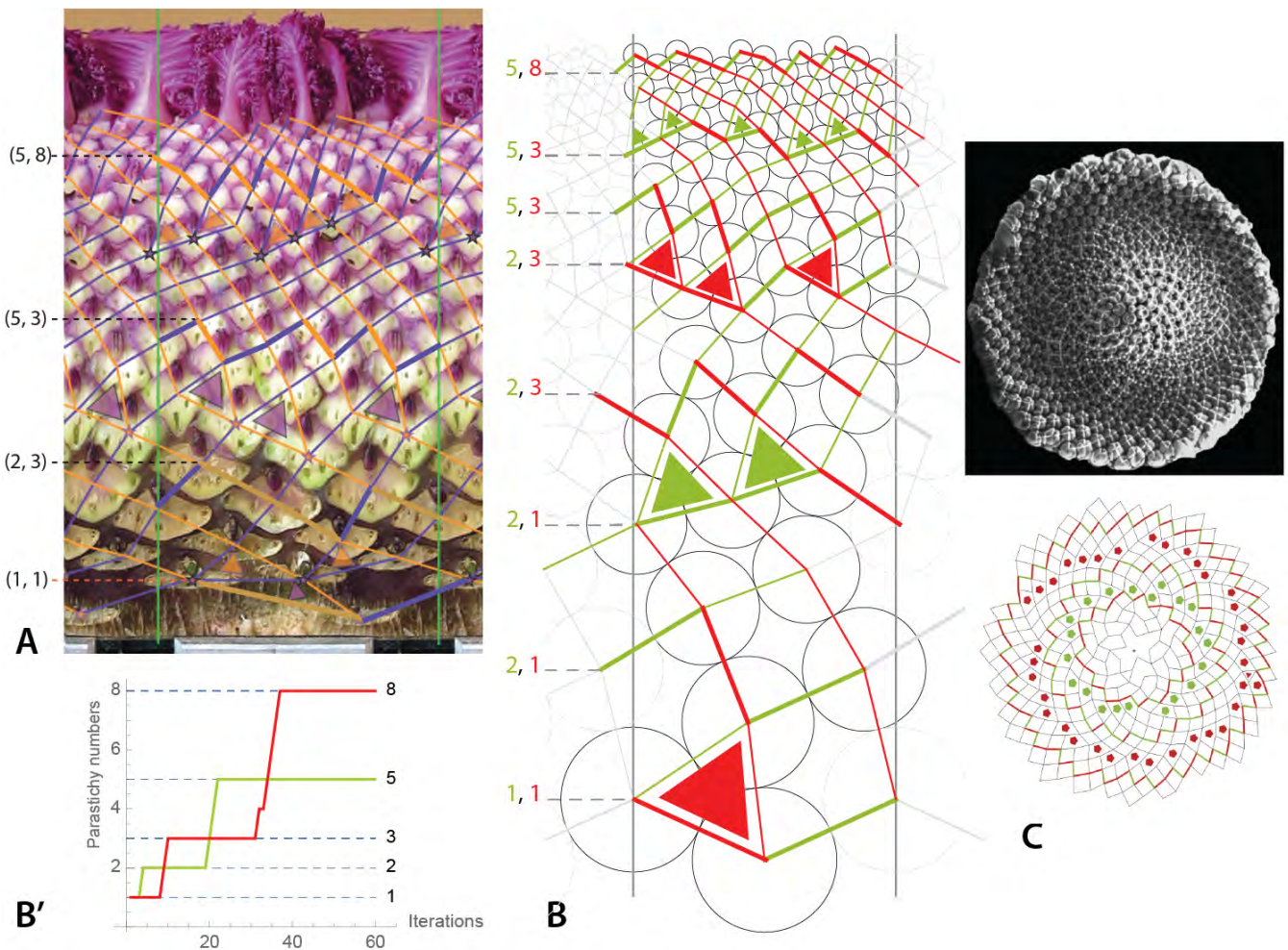
Figure 9: **Fibonacci transitions in vivo and in silico.** (A) Unrolled ornamental cabbage with removed leaves. The pattern of line segments joining adjacent leaf scars, shows a sequence of Fibonacci transitions from (1, 1) to (5, 8) via a succession of clusters of triangle transitions that alternate sides. (B) Although no attempt was made to exactly match the cabbage pattern, this computer simulation, where the diameter $d$ of the disks decreases linearly with their height, shows the same alternating pattern of triangle transitions between (1, 1) and (5, 8). (B') Graph of front parastichy numbers as function of the number of iterations, from the simulation in (B), showing the red and green parastichy numbers monotonically increase one by one to the sum of the previous two. This is a signature of a regular Fibonacci transitions, easily detectable in computer simulations. (C) Filled in meristem of an artichoke meristem (SEM courtesy J. Dumais). Three concentric fronts are shown on the right, with parastichy numbers (34, 55), (34, 21), and (13, 21) transitioning via pentagons as one moves closer to the center.
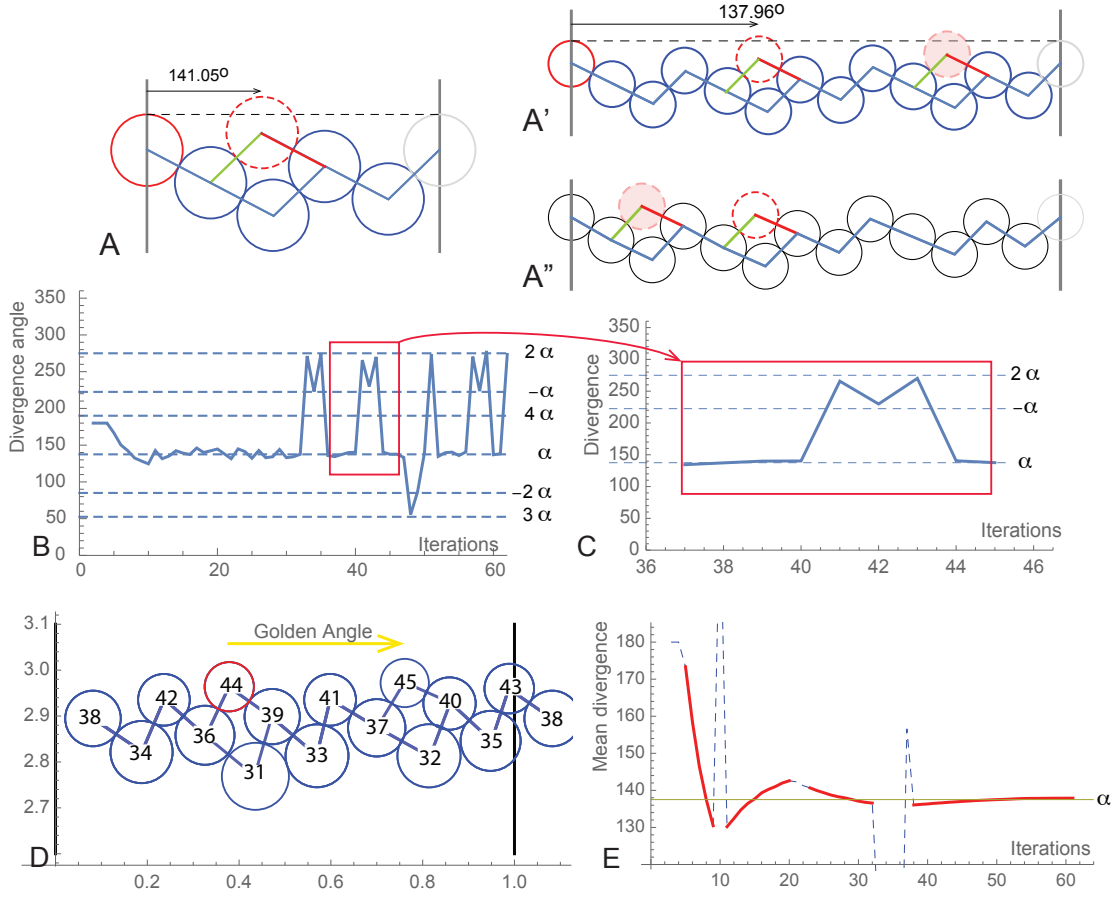
21

Figure 10: **Fronts and angle of divergence.(A & A')** (3,2) and (8, 5) fronts (blue), and their child disks (dashed) show the emergence of the golden angle, as their parastichy numbers increase through the Fibonacci sequence. These fronts, extracted from rhombic lattices, have each identical up and identical down segments. **(A")** A slight perturbation of the front in A' results in a change in the order of initiation of primordia: whereas the divergence for the first and second new disk was roughly $\gamma$ in A', it is close to $\gamma$ and $2\gamma$ in this case **(B)** Angle of divergence at each iteration of the simulation of Figure 9.B. While at first the angle seems to converge towards the golden angle $\alpha$, it then starts oscillating widely. However the values it hits are all close to multiples of $\alpha$. This is explained by permutations of the vertical order of the disks, as in A". **(D)** Simulation with disks of decreasing size showing an instance of a permutation, where the angle between disks 38 and 39, 39 and 40 are very close to $\alpha$, but disks 41 and 42 are switched as compared to the order of regular fronts. **(E)** These permutations are averaged out when taking the mean of the divergence angle over a front: in the right coordinate frame, the red curve in this graph espouses closely the Fibonacci branch of the van Iterson diagram of Fig. 7. The blue dashed lines correspond to triangle transitions.

Fortunately, this noise appears to be smoothed out during further decrease of the growth index, while staying in the same mode, leading to global stability. This mechanism is thus robust to extrinsic noise as much as it is robust even to the noise it spontaneously generates itself.

**When the patterns is not Fibonacci.** What happens when the conditions (regularity of fronts, slow decrease of $G$) for Fibonacci phyllotaxis morphogenesis fail? As seen in Fig. 8, one of the important consequences of regularity and slow decrease of $d$ is that in a $(i, j)$ front with $i > j$, the $j$ down segments are *all* steeper than each of the $i$ up segments.

As a consequence, when the triangle transitions occur, as they must, they do so exclusively on the up segments - and the roles are reversed for the next set of transitions. This uniform difference of steepness between up and down segments is lost when $G = d/D$ is rapidly decreased. In this case triangle transitions happen often on the up *and* down segments one after the other. The net effect of this type of growth is that the parastichy numbers will keep close to one another.

If $G$ is kept constant, a pattern starting with an irregular front will have the tendency, via pairs of triangle and pentagon transitions, to regularize and its parastichy numbers will tend to get closer to one another. Both these phenomena, are on display in the simulation of Fig. 11 A, B and C. The latter phenomenon of convergence is shown in the male cone of a Cedar of Lebanon for example (Figs. 1.A right and 11 A). Because the parastichy numbers are close in these patterns, and their parastichy (when visible) have symmetric slopes, we call these patterns *quasi-symmetric*(Golé et al. 2016, Douady & Golé 2017). Aside from the Cedar of Lebanon, we have found them in many samples of inflorescence that undergo a rapid expansion from the stem: corn, strawberries, peace Lily. Work in progress shows that these inflorescences have statistically different phyllotaxis than Fibonacci or any Fibonacci-like pattern (e.g. Lucas or multijugate). They are also statistically distinguishable from whorled patterns.

Note that the evolution of the parastichy numbers in the development of a quasi-symmetric pattern is structurally different from the Fibonacci-like case, and the attempt of classifying a (4, 5) pattern, for instance, as part of a sequence 1, 4, 5, 9, 14... is futile, and misleading: the quasi-symmetric pattern will most likely *not* evolve in these higher modes, nor will it necessarily converge to a (4, 4) or (5,5) whorled-pattern.

# 6    Discussion

**Phyllotaxis as a conspicuous example of developmental canalization.** Organ initiation rules in SAM and fronts provide a simple explanation of the nature of developmental constraints at the origin of phyllotaxis process in plants. Contrary to what was believed in the first place (for instance by the Bravais brothers), developmental constraints apply locally to parastichies, which in turn determine the mean divergence angle (and not the other way around!). This is due to the fact that all lateral organs in plant stems, be they part of compressed or elongated structures, are initiated in a tiny region at the SAM where competition for space is the rule. There, the patterning is dominated by the opportunistic initiation of organs as the initiation zone progressively moves away from the already initiated organs. This process itself is governed by the geometric arrangement of recently initiated organs (the fronts) and by the plant growth (the parameter $G = d/D$). During stem growth, phyllotaxis is thus progressively canalized from a $(1, 1)$ front with divergence angle of $180^o$, or a $1/2$ turn to higher order Fibonacci fronts with average divergence angles that converge to the golden angle. These features emerge from the inhibition- and growth- based iterative process of primordia formation, as it is canalized from a Fibonacci front to the next, at least as the growth parameter $G$ decreases slowly. The system starting with an angle of $1/2$ a turn between the first two primordia, progressively imposes the coarser convergent of the divergence angle: $1/2$ then $1/3$.
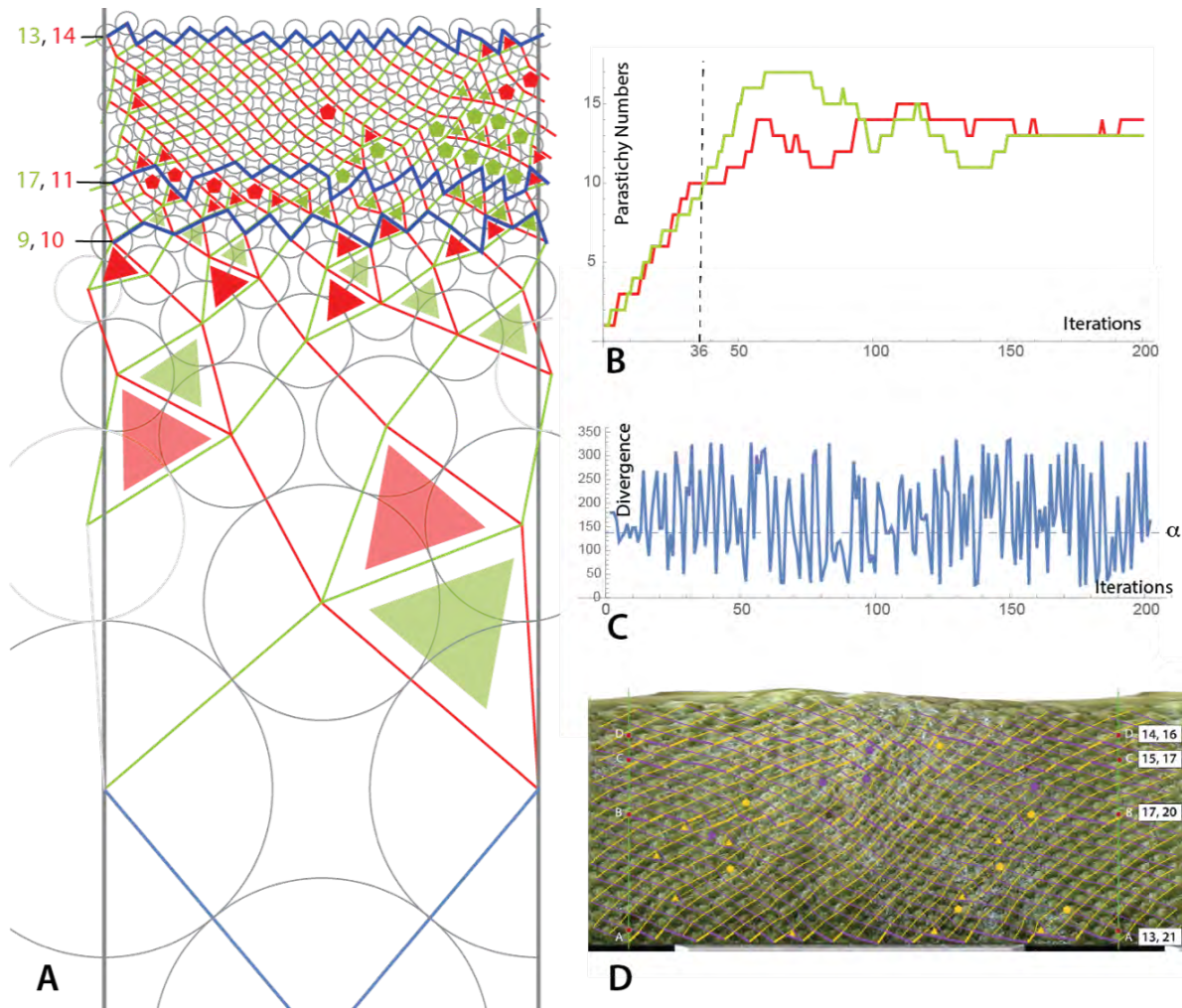
Figure 11: **Quasi symmetry in vivo and in silico.** **(A)** 200 iteration of the stacking process starting from a (1,1) front. The parameter $d$ was rapidly decreased, linearly with height, until iteration 36, where the pattern reaches a (9, 10)-front. After that $d$ was kept constant. Note the erratic occurrences of both red and green triangle transitions with no real separation between them. After iteration 36, the pattern converges erratically to 13, 14 fronts, somewhat stabilized by pentagon transitions, paired with triangles. **(B)** The parastichy number graphs show the almost simultaneous increase of the two parastichy numbers up to iteration 36, and their convergence to 13,14 after that. **(C)** The divergence angle, similarly irregular, has nothing to do with the golden angle anymore. **(D)** *Cedrus libani* male cone, exhibiting a transition from an irregular Fibonacci (13,21) front to the quasi symmetric (14,16), via a combination of triangle and pentagon transitions.

24

Any divergence angle that would have both 1/2 and 1/3 as its first convergents would then be consistent with the pattern. The precise angle is determined by the rate of increase of the central zone, *i.e.* $D$ (or equivalently the rate of decrease of the organ size relative to the center size, *i.e.* $G$) and by intrinsic biological variability. Then, as growth continues and the size of the disks decreases, Fibonacci modes augment due to the fronts' Fibonacci adding property and new convergents are imposed to the divergence angle that have average values close to 2/5, then 3/8, 5/13, etc., thus imposing progressively and more and more precisely a range of divergence angles that converges on average towards the theoretical Golden angle, while never exactly reaching it. For high order modes, this process traps the divergence angle, keeping it close to a multiple of the golden angle with an amazing precision, but only *in average*. This multiscale canalization process is particularly robust as the fronts can produce many values of divergence angles at the microscopic level without modifying the macroscopic patterns (the parastichies).

**Is the golden angle a trait of high fitness value for natural selection ?** We showed in the section 3 that a divergence angle equal to the golden angle would automatically give rise to Fibonacci spirals. This is essentially what the Bravais brothers discovered early on in 1835 (Bravais & Bravais 1837). More precisely, the Bravais brothers showed that if the divergence angle is the golden angle, then we always see two system of parastichies, no straight arms, and the parastichy numbers will be always two consecutive numbers of the Fibonacci sequence. For large growth index $G$, one would see only few spirals, but for smaller and smaller ones, one observes larger and larger numbers of spirals, always two consecutive Fibonacci numbers.

This striking property motivated them to propose that the divergence angle would be selected to be equal to this golden angle in plants, and that it would be the explanation of the observation of these consecutive Fibonacci numbers of parastichies. This view is still largely prevalent nowadays. One reason for that is its simplicity, were everything depends only on one parameter, the divergence, being fixed at a very particular value. Moreover, the fact that this value possesses many mathematical properties is commonly viewed as a reason for its natural selection, despite the weaknesses of the arguments explaining why such properties should provide plants with higher fitness values. For instance the fact that it is an irrational value the furthest away from the rationals is still often quoted as ensuring that two leaves never superpose exactly, so they do not shadow each other, which would be favourably selected. However this argument has some weaknesses: although some simulations show that in some ideal (unrealistic) cases the golden angle may provide optimum insolation to the leaves, many other angles provide the same maximal amount, and this preference can be undone by varying the shape of the leaves, (Strauss et al. 2019). And this does not take into account the fact that the leaves orient themselves after being initiated, turning toward the light, independently of their insertion on the stem, nor the fact that there are many plants with perfectly superposed leaves such as in many whorled plants, e.g Hebe in 1.B, and that have however managed to make it through in the struggle for life.

**Divergence, an ill-defined concept.** Since the beginning of the quantitative research on phyllotaxis, divergence has been a convenient concept to think about phyllotaxis and its models. However, in the recent years, it has increasingly appeared as a ill-defined concept. First, divergence is difficult to measure if not impossible. Most of the time, based on the assumption that it represents a real factor in pattern formation and that a clear order between primordia initiation exists, it is estimated as the average over indirect measurements (either at macroscopic or at microscopic levels). However, it has been observed in various recent works, either in real plants or in simulations that the angle between successive primordia (i.e. the divergence angle) is rather a multiple of a specific angle. The divergence is therefore not constant in these systems. Rather, at every moment, this angle is imposed by the existing primordia fronts and by the size of the initiated organs. The divergence corresponds in this

viewpoint to a spatial (angular) period in the initiation of the organs, for which the order (and thus plastochrone) can markedly vary. The divergence would then more consistently be defined as a mean angle between two consecutively initiated organs over a period of the pattern, consistently with the fact that the spatial patterns mainly remain unaffected even if the timing of initiation markedly fluctuates. It is this mean divergence angle, visible in the spatial period of the lattice, that is progressively canalized during growth, by reduction of the growth index, towards the Golden angle.

**Justification of canalization.** The scientific history of phyllotaxis shows how difficult it is to explore morphogenesis. The first difficulty is to characterise the shape of the prototypical patterns whose formation one studies (*i.e.* lattices in our case). Even in the relatively simple and striking case of phyllotaxis, it took mankind till the turn of the $19^{th}$ century to recognize these patterns. Then, once the necessarily simplistic description is obtained, it is tempting to reverse cause and effect, and to think that what is observed is the result of our abstract description. In phyllotaxis, the selection of a particular divergence angle was instituted as the cause for Fibonacci phyllotaxis, rather than as an emerging effect of a localized morphogenetic mechanism. This common inversion of cause and effect may become irresistible if the description we discover has some profound and rich mathematical properties (*e.g.* the van Iterson diagram and its beautiful number theory based symmetry). The temptation is great to think that these deep, unifying properties are the reason behind the observations.

One has to make a real effort then to go back to the actual biological and physical constraints that participate in building the shape, and to figure out how they play out in the geometry of the morphogenetic mechanism[6]. In phyllotaxis, the constraints come from the local conditions of growth of a new organ (*e.g.*, local accumulation of auxin, inhibition of growth in surrounding areas). Even in realistic noisy situations, these conditions are still surprisingly capable of producing results that are close to the perfect abstract case (*e.g.* lattice). But when the noise is too large, and variation too abrupt, they produce cases (*e.g.* quasi-symmetry) which are indeed observed in plants, but were overlooked because not neatly fitting in the polished descriptive framework.

**Restating the central question of phyllotaxis.** To proceed further in the direction pointed to here, it seems important to scrutinize the precise dynamics of organ growth, as it is probably one of the key components to the selection of phyllotaxis patterns. For instance, is it true that the future pattern is determined by the configuration of the latest front of primordia, and the variations of the growth index through time? And if so, is it possible to measure precisely the history of fronts in different cases of transitions, leading to both Fibonacci or quasi-symmetric patterns, and compare this data with results from the models? Are the observed growth dynamics comparable? Once this quantitative connection between model and reality is secured, the central question of the predominance of Fibonacci phyllotaxis would then be: why do plants select a history of variation of growth rate slow enough to give rise to these patterns?

**Coda.** In conclusion, the Bravais brothers were right about at least one thing: the hypothesis of the divergence angle being constant (and usually equal to the golden angle) did serve as a useful guide to the study of phyllotaxis. A canalization, as it were, of the scientific discourse through time, oscillating between partial rejection and partial acceptance of this hypothesis, between its role as cause or as effect.

---

[6]This point of view was already expressed by Schwendener in 1868, when he contrasted his approach to that of Schimper and Braun, whose work, he contended, "is founded on an idealistic view of nature in which forms of organs follow ever-existing patterns and structures. Consequently, their [spiral] theory doesn't rely on dynamic principles to explain the design mechanisms of plants."

# References

Adler, I. (1974), 'A model of contact pressure in phyllotaxis', Journal of Theoretical Biology **45**, 1–79.

Alberch, P. (1982), Developmental Constraints in Evolutionary Processes, in 'Evolution and Development', Springer, Berlin, Heidelberg, pp. 313–332.

Alberch, P. (1991), 'From genes to phenotype: dynamical systems and evolvability', Genetica **84**(1), 5–11.

Atela, Golé & Hotton (2003), 'A Dynamical System for Plant Pattern Formation: A Rigorous Analysis', Journal of Nonlinear Science **12**(6), 641–676.

Atela, P. (2011), 'The Geometric and Dynamic Essence of Phyllotaxis', Mathematical Modelling of Natural Phenomena **6**(2), 173–186.

Atela, P. & Golé, C. (2007), 'Rhombic tilings and primordia fronts of phyllotaxis (preprint)'. http://arxiv.org/abs/1701.01361.

Barbier de Reuille, P., Bohn-Courseau, I., Ljung, K., Morin, H., Carraro, N., Godin, C. & Traas, J. (2006), 'Computer simulations reveal properties of the cell-cell signaling network at the shoot apex in Arabidopsis.', Proceedings of the National Academy of Sciences **103**(5), 1627–1632.

Battjes, J., Vischer, N. & Bachmann, K. (1993), 'Capitulum Phyllotaxis and Numerical Canalization in Microseris-Pygmaea (Asteraceae, Lactuceae)', American journal of botany **80**(4), 419–428.

Besnard, F., Refahi, Y., Morin, V., Marteaux, B., Brunoud, G., Chambrier, P., Rozier, F., Mirabet, V., Legrand, J., Lainé, S., Thévenon, E., Farcot, E., Cellier, C., Das, P., Bishopp, A., Dumas, R., Parcy, F., Helariutta, Y., Boudaoud, A., Godin, C., Traas, J., Guédon, Y. & Vernoux, T. (2014), 'Cytokinin signalling inhibitory fields provide robustness to phyllotaxis.', Nature **505**(7483), 417–421.

Braun, A. (1831), 'Vergleichende Untersuchung über die Ordung der Schupper an den Tannenzapfen, als Einleitung zur Untersuchung der Blattstellung überhaupt', Nova Acta Physico-Medica **XV**, 191–403.

Bravais, L. & Bravais, A. (1837), 'Essai sur la disposition des feuilles curvisériées', Ann. Sci. Nat. **7**, 42–110.

Couder, Y. (1998), 'Initial transitions, order and disorder in phyllotactic patterns: the ontogeny of Helianthus annuus: a case study', Acta societatis botanicorum Poloniae **67**(2), 129–150.

Debat, V. & Le Rouzic, A. (2019), 'Canalization, a central concept in biology', Seminars in Cell & Developmental Biology **88**, 1–3.

Douady, S. & Couder, Y. (1992), 'Phyllotaxis as a physical self-organized growth process.', Physical review letters **68**(13), 2098–2101.

Douady, S. & Couder, Y. (1996a), 'Phyllotaxis as a dynamical self organizing process. Part I: The spiral modes resulting from time-periodic Iterations', Journal of Theoretical Biology **178**, 255–274.

Douady, S. & Couder, Y. (1996b), 'Phyllotaxis as a dynamical self organizing process. Part III: The simulation of the transient regimes of ontogeny', Journal of Theoretical Biology **178**(3), 295–312.

Douady, S. & Golé, C. (2017), ' Fibonacci or Quasi-Symmetric Phyllotaxis, Part II : Botanical Observations', Acta societatis botanicorum Poloniae **This special issue**.

Félix, M.-A. & Barkoulas, M. (2015), 'Pervasive robustness in biological systems', Nat Rev Genet **16**(8), 483–496.

Fierz, V. (2015), 'Aberrant phyllotactic patterns in cones of some conifers: a quantitative study', Acta Societatis Botanicorum Poloniae **84**(2).

Galvan-Ampudia, C. S., Chaumeret, A. M., Godin, C. & Vernoux, T. (2016), 'Phyllotaxis: from patterns of organogenesis at the meristem to shoot architecture', Wiley Interdisciplinary Reviews: Developmental Biology **5**(4), 460–473.

Golé, C. & Douady, S. (2019), 'Convergence of a disk stacking process on the cylinder (preprint)'. http://arxiv.org/.

Golé, C., Dumais, J. & Douady, S. (2016), 'Fibonacci or quasi-symmetric phyllotaxis. Part I: why?', Acta societatis botanicorum Poloniae **85**(4), 1–34.

Hofmeister, W. (1868), Allgemeine morphologie der gewashe, in 'Handbuch der Physiologischen Botanik', Engelmann, pp. 405–664.

Hotton, S., Johnson, V., Wilbarger, J., Zwieniecki, K., Atela, P., Golé, C. & Dumais, J. (2006), 'The possible and the actual in phyllotaxis: Bridging the gap between empirical observations and iterative models', Journal of Plant Growth Regulation **25**(4), 313–323.

Huether, C. A. (1968), 'Exposure of natural genetic variability underlying the pentamerous corolla constancy in Linanthus androsaceus ssp. androsaceus.', Genetics **60**(1), 123–146.

Karpenkov, O. (2013), Geometry of Continued Fractions, Vol. 26 of Algorithms and Computation in Mathematics, Springer-Verlag.

Livio, M. (2008), The Golden Ratio, The Story of PHI, the World's Most Astonishing Number, Broadway Books.

Maynard Smith, J., Burian, R., Kauffman, S., Alberch, P., Campbell, J., Goodwin, B., Lande, R., Raup, D. & Wolpert, L. (1985), 'Developmental Constraints and Evolution: A Perspective from the Mountain Lake Conference on Development and Evolution', The Quarterly Review of Biology **60**(3), 265–287.

Mitchison, G. J. (1977), 'Phyllotaxis and the fibonacci series.', Science **196**(4287), 270–275.

Pennybacker, M., Shipman, P. & Newell, A. (2015), 'Phyllotaxis: Some progress, but a story far from over', Physica D: Nonlinear Phenomena **306**, 48–81.

Plantefol, L. (1948), La théorie des hélices foliaires multiples, Masson.

Prusinkiewicz, P. & Lindenmayer, A. (1990), The algorithmic beauty of plants, Springer.

Refahi, Y., Brunoud, G., Farcot, E., Jean-Marie, A., Pulkkinen, M., Vernoux, T. & Godin, C. (2016), 'A stochastic multicellular model identifies biological watermarks from disorders in self-organized patterns of phyllotaxis.', eLife **5**, 231.

Reinhardt, D., Pesce, E.-R. R., Stieger, P., Mandel, T., Baltensperger, K., Bennett, M., Traas, J., Friml, J. i. & Kuhlemeier, C. (2003), 'Regulation of phyllotaxis by polar auxin transport.', Nature **426**(6964), 255–260.

Richards, F. J. (1951), 'Phyllotaxis: Its Quantitative Expression and Relation to Growth in the Apex', Philos Trans R Soc Lond B Biol Sci **235**(629), 509–564.

Schimper, K. F. (1835), 'Beschreibung des symphytum zeyheri und seiner zwei deutschen verwandten der s. bulbosum schimper und s. tuberosum jacq.', Geigers Magazin für Pharmacie **29**, 192.

Schwendener, S. (1878), Mechanische Theorie der Blattstellungen, W. Engelmann, Leipzig.

Smith, R. S. & Prusinkiewicz, P. (2006), 'Inhibition fields for phyllotactic pattern formation: a simulation study', Canadian Journal of Botany **84**(11), 1635–1649.

Snow, M. & Snow, R. (1952), 'Minimum areas and leaf determination', Proceedings of the Royal Society of London B: Biological Sciences **139**(897), 545–566.

Strauss, S., Lempe, J., Prusinkiewicz, P., Tsiantis, M. & Smith, R. S. (2019), 'Phyllotaxis: is the golden angle optimal for light capture?', New Phytologist .

Swinton, J., Ochu, E. & Consortium, M. T. S. (2016), 'Novel fibonacci and non-fibonacci structure in the sunflower: results of a citizen science experiment', Royal Society open science **3**(5), 160091.

Van Iterson, G. (1907), 'Mathematische und microscopisch-anatamische studien uber blattstellungen, nebst betraschungen uber der schalenbau der miliolinen gustav-fischer-verlag', G. Fischer: Jena . available online through google books.

Veen, A. (1973), 'A computer model for phyllotaxis. a network of automata'.

Vlot, E. C. & Bachmann, K. (1991), 'Genetic and Non-genetic Variation in the Number of Pappus Parts in Microseris douglasii Strain D37 (Asteraceae, Lactuceae)', Annals of Botany (68), 235–241.

**Box 1 - Fibonacci maths: a (minimal) digest**

**Fibonacci sequence.** In mathematics, the celebrated Fibonacci sequence is defined as the sequence of integers:

$$1, 1, 2, 3, 5, 8, 13, 21, 34, 55, 89, 144, \ldots,$$

where the first two terms, 1 and 1, are given and any term of rank greater than 2 is defined as the sum of the two preceding ones, e.g. $89 = 34 + 55$. If $F_n$ denotes the $n$th term, the sequence can be compactly defined as:

$$F_1 = 1, F_2 = 1,$$
$$F_{n+1} = F_n + F_{n-1}. \tag{1}$$

Related sequences can be constructed based on the same rule by changing the two initial terms. For example, by changing the first two terms to 1 and 3, one gets the Lucas sequence:

$$1, 3, 4, 7, 11, 18, 29, 47, 76, 123, \ldots.$$

The Fibonacci sequence has a number of remarkable mathematical properties. A key property related to phyllotaxis stems from the sequence of ratios of consecutive terms of the Fibonacci sequence:

$$\frac{1}{1}, \frac{2}{1}, \frac{3}{2}, \frac{5}{3}, \frac{8}{5}, \frac{13}{8}, \frac{21}{13}, \frac{34}{21}, \frac{55}{34}, \frac{89}{55}, \frac{144}{89}, \ldots. \tag{2}$$

In decimal notation, this writes as (numbers given with a $10^{-4}$ precision):

$$1.0, 2.0, 1.5, 1.6667, 1.6, 1.625, 1.6154,$$
$$1.6191, 1.6178, 1.6182, 1.6180, \ldots,$$

showing that the consecutive values get closer and closer and seem to converge toward a particular real number. It can be easily shown using eq. 1 that this is indeed the case and that this number is the *golden number* $\phi = 1.61803\ldots$. Even starting with different initial numbers, the Lucas sequence shows the same property, i.e. that the ratio of two consecutive numbers tends toward the golden number.

**The Golden number.** The golden number is defined as:

$$\phi = \frac{1 + \sqrt{5}}{2} = 1.61803\ldots.$$

This celebrated irrational number has a simple geometric interpretation. Let us consider a straight segment of unit length. We wonder how to divide this segment into two parts of length $x$ for the largest segment and $1 - x$ for the smallest such that relative length proportions remain constant from one segment to the next (i.e. from $1 - x$ to $x$ and from $x$ to 1), Fig A. This can be expressed as:

$$\frac{1}{x} = \frac{x}{1 - x}. \tag{3}$$
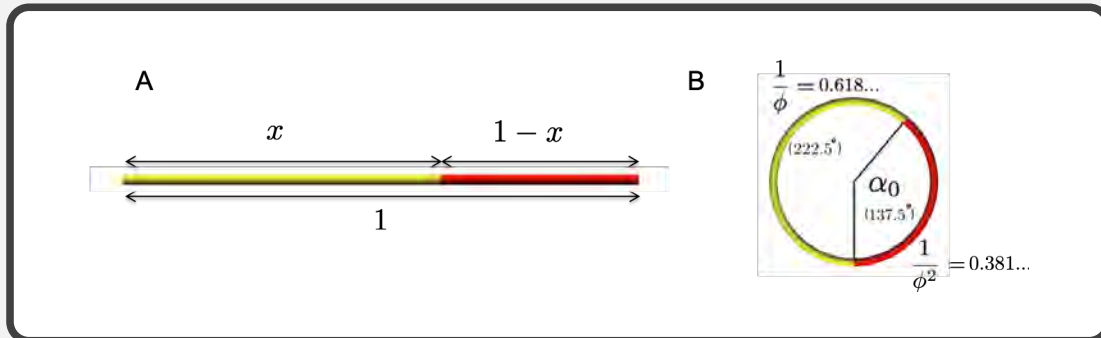
This thus leads us to solve a quadratic equation whose unique positive solution is:

$$x = \frac{\sqrt{5}-1}{2} = 0.618\ldots.$$

Simple algebra shows that proportion $\frac{1}{x}$ between the 3 consecutive segments defined by eq. (3) is just $\phi$:

$$\frac{1}{x} = \frac{2}{\sqrt{5}-1} = \frac{1+\sqrt{5}}{2} = \phi.$$

Due to its ability to preserve proportions while scaling, $\phi$ has been called the *golden ratio* and can be found in various human creations (e.g. (Livio 2008)). Interestingly, $\phi$ verifies a number of remarkable identities that can be derived from 3. For example its inverse is $\phi - 1$:

$$\phi(\phi - 1) = 1. \qquad (4)$$

The length of the two segments can then be expressed in term of $\phi$:

$$x = \frac{1}{\phi}, \qquad (5)$$

$$1 - x = 1 - \frac{1}{\phi} = \frac{\phi - 1}{\phi} = \frac{1}{\phi^2}, \qquad (6)$$

leading to approximated values $x = 0.618$ and $1 - x = 0.382$.

**The Golden angle.** The golden angle is simply derived from the golden number by subdividing a circle of perimeter 1 unit into two circular segments of length $x$ and $1 - x$ verifying the same geometrical constraints as expressed in eq. 3, Fig. B. By a similar reasoning, we find that $x = \frac{1}{\phi}$ and $1 - x = \frac{1}{\phi^2}$. The golden angle, denoted $\gamma$, is then simply the angle that intercepts the smaller perimeter segment (of length $1-x$). Its value is thus:

$$\gamma = \frac{1}{\phi^2} = 2 - \phi = \frac{3 - \sqrt{5}}{2} \qquad (7)$$

In radians, the golden angle value is thus:

$$\gamma = 2\pi\phi^{-2} = 2\pi\,0.382 = 2.4 \text{ rad.} \qquad (8)$$

Converted in degrees it yields:

$$\gamma = 360°\phi^{-2} \approx 137.51°.$$

## Box 2: Best rational approximation of a real number with pieces of size $1/q$

Imagine that we cut a pie into 8 pieces (sectors) of equal size (Fig. A) and that a guest wishes to get $1/3$ of the pie. We assume that we have no other means than offering him a number of the already cut pieces of size $1/8$ (we cannot cut the initial pieces into smaller pieces).
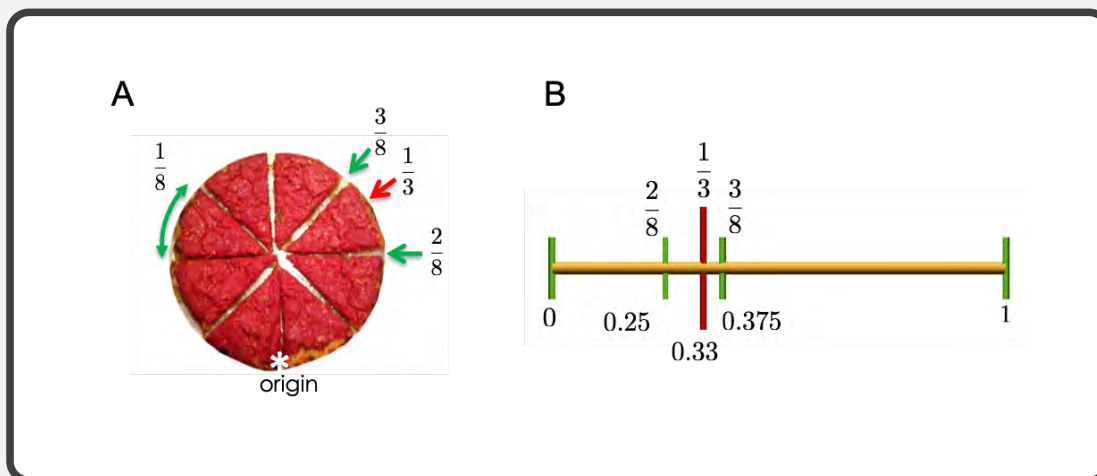


To best fit our guest wish, it is obvious that we must give her either 2 or 3 pieces. To make the decision between these two options, we compare them more precisely to the actual guest demand of $1/3$. 2 pieces, i.e. $2/8$, is 0.25 while 3 pieces, i.e. $3/8$, is 0.375. As 0.375 is closer to $1/3 = 0.333$ than 0.25, we finally find it more reasonable to give her 3 sectors. We can say that $3/8$ is the best way to approximate our given target number (here $1/3$), with pieces of size $1/8$, (Fig. B).

Likewise, it is possible for each positive real number $\alpha \leq 1$ to find the best approximation of this number with pieces of size $1/q$, $q$ being an integer ($q = 8$ in the previous example). Note that $p \leq q$ as, by trying different values $p = 0, 1, 2, ...$, all the possibilities of approaching $\alpha \leq 1$ have been explored, as soon as $p = q$. The higher $q$, the smaller the piece. For each value of $q$, there exists a number of pieces $p$ such that $p.\frac{1}{q}$ best approximates our target number $\alpha$ ($p = 3$ in the previous example). The fraction $\frac{p}{q}$ is called **the best rational approximation of $\alpha$ with pieces of size $\frac{1}{q}$**. Among the best rational approximations of a number, some are best rational approximations in a stronger sense: they are called the strong best rational approximations of this number (See Supplementary Information section 2 for mathematical details about best rational approximations of reals and for the companion notion of *strong best approximations*). These strong best rational approximations are the *convergents* of this number.

One classical way to obtain the convergents of a real number $\alpha$ is by expressing $\alpha$ as a *continued fraction*. In our example:

$$\alpha = \frac{41}{100} = \cfrac{1}{2 + \cfrac{1}{2 + \cfrac{1}{3 + \cfrac{1}{1 + \cfrac{1}{1 + \cfrac{1}{2}}}}}}$$

(see Supplementary information Section 3 on how to derive the continuous fraction of a real). The convergents are then just the successive truncations of that contin-ued fraction. For instance,

$$\frac{2}{5} = \cfrac{1}{2 + \cfrac{1}{2}}, \quad \frac{7}{17} = \cfrac{1}{2 + \cfrac{1}{2 + \cfrac{1}{3}}},$$

$$\frac{9}{22} = \cfrac{1}{2 + \cfrac{1}{2 + \cfrac{1}{3 + \cfrac{1}{1}}}}, etc.$$

If $\alpha$ is rational, it has a finite continued fraction expansion, and therefore a finite number of convergents (the last convergent being $\alpha$ itself). But if $\alpha$ is irrational, the continued fraction continues for ever and $\alpha$ has consequently an infinite number of convergents.

If we assume that a spiral motif was created with a constant divergence angle (as with our simple geometric model), the previous analysis makes it possible to derive information about the divergence angle from the observation of spiral motifs.

Let us illustrate how this works on an example. Imagine that we have a pinecone with (8,13) phyllotaxis as in the following figure.
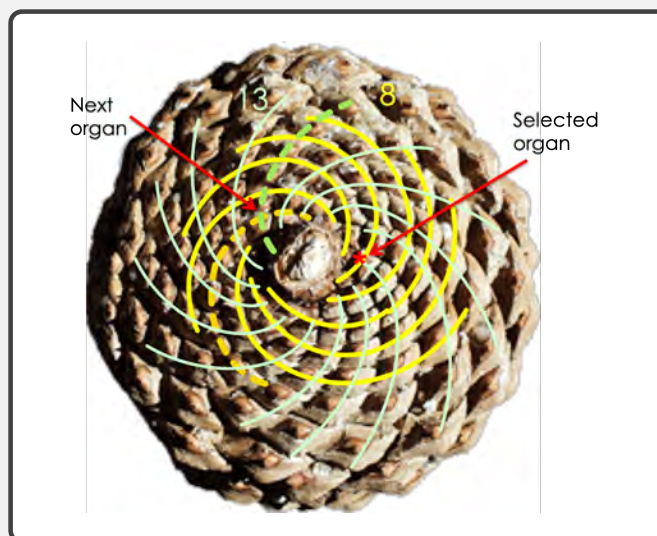
According to the previous analysis, here is what can be deduced from this spiral organization:

1. Spirals are the traces of fractional approximations of the divergence angle (assumed constant in time).

2. The accuracy of this approximation relies on the size of organs: the smaller the organs the more precise the approximation.

3. 8 and 13 being two consecutive numbers in the Fibonacci sequence, the divergence angle is comprised between two convergents of the Golden angle.

4. More precisely, the divergence angle is comprised between $3/8$ and $5/13$. Indeed we know that 8 and 13 are necessarily denominators of a pair of consecutive convergents of the divergence angle (fractions that best approximate the divergence angle at a precision imposed by organ size). One of these fractions approaches the divergence angle from below while the other approaches it from above (the convergents are alternating around their target). These convergents are of the form $F_{n-2}/F_n$, leading to the two angles: $3/8 = 0.375$ ($135°$) and $5/13 = 0.385$ ($138.6°$).

5. For a chosen initial organ, the next organ is approximately at $3 \times 1/8$ turns from the initial organ. This means that this organ lies somewhere on the 3rd spiral arm of 8-arms family, starting from the arm the initial organ belongs to and going either clockwise or counter-clockwise. Similarly the next organ is also approximately at $5 \times 1/13$ turns from the initial organ modulo 1 turn in the same direction. This determinates the position of 2 potential next organs (depending on whether we counted spirals clockwise or counter-clockwise). The next initiated organ is the one is then at the intersection of the two spirals, and that is farthest away from the center (heree at the intersection of the two dashed spirals). One can observe that the angle is as expected close to $137°$.

Another way to find the organ succeeding a given one is to notice that in a regular pattern, the initiation number of a primordia increase by the number of spirals along a parastichy this give the property that the element in the diagonal (orthostichy) has a number sum of the number of spirals. Using this property all the elements can be numbered one by one by local spiral connections, and then eventually the whole pattern can be numbered. Then the divergence angle can be measured. The spirals thus create a reference system when one can recover the exact ordering and position of every organ.

## Box 5: The Fibonacci rule along the diagram
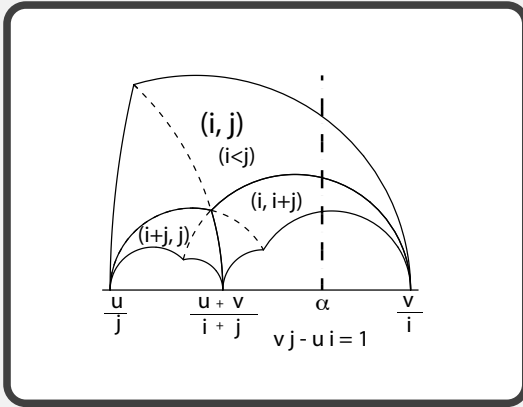


In the diagram of Fig 7, it turns out that, immediately under each quadrilateral region of mode $(i, j)$, there are two regions of modes $(i+j, j)$ and $(i, i+j)$ (Atela et al. 2003), see figure above. This makes intuitive sense: if in the lattice points $i$ and $j$ are closest to the reference point 0, then by symmetry, point $i + j$ is closest to both of them. Traveling down in the $(\alpha, T)$ plane along the branch of the van Iterson diagram in region $(i, j)$ (dashed line in the figure above), as one crosses the vertex at the bottom of the branch, the point $i + j$ becomes one of the closest two to point 0. One of the sets of $i$ or $j$ contact parastichies is then replaced by the new one, $i + j$. But which of the two? Remarkably, the choice compatible with the stacking process is always so that one goes from mode $(i, j)$ to mode $(i, i+j)$ (if $i > j$) or $(i+j, j)$ (if $i < j$). But this is the Fibonacci rule! Take for example $(i, j) = (3, 5)$. Then $3 = i < j = 5$, so the next mode compatible with the stacking process is $(i + j, j) = (8, 5)$. In general a mode of two consecutive Fibonacci numbers gives rise to a mode with the next two consecutive numbers. The rejected choice yields lattices with the two sets of parastichies winding in the same direction, which is incompatible with the stacking process, as parents are always on the opposite sides of the child disk. This explains the "pruned" branches of the van Iterson diagram in Figure 8.

Traveling down the van Iterson diagram from its top $(1, 1)$ branch, one has to first make a choice of going left in the $(2,1)$ region or right in the $(1,2)$ region - this choice will determine the chirality of the pattern. Say we go left, decreasing of $T$ while varying $\alpha$ to keep the lattice rhombic will lead us down through region of successive Fibonacci modes. While $\alpha$ has to oscillate back and forth to keep the lattice rhombic, it does so with less and less amplitude as it converges to the point $(\gamma, 0)$ on the $\alpha$-axis.

**Convergents, revisited.** The figure above also shows visually the correspondence between rational approximations of a divergence angle and the parastichy numbers in this cylindrical model. Indeed one can show that the two "foot" points on the $\alpha$ axis of region of mode $(i, j)$ are $\frac{u}{j}$ and $\frac{v}{i}$ where $u, v$ are such that $vj - ui = \pm 1$ and $0 < v \le i, 0 < u \le j$ (see the figure above). As a result, if a lattice of divergence angle $\alpha$ is in mode $(i, j)$, $\frac{u}{j}$ and $\frac{v}{i}$ are the best approximation using pieces of size $i$ and $j$ respectively of $\alpha$ (As we know, these best approximation fractions include in particular all the convergents of $\alpha$). Conversely, if an angle $\alpha$ is between two rationals $\frac{u}{j}$ and $\frac{v}{i}$ where $ui - vj = \pm 1, 0 < v \le i, 0 < u \le j$, the lattice given by $(\alpha, T)$ *must* have parastichy numbers $(i, j)$ for *some* range of $T$: the vertical line for that value of $\alpha$ necessarily crosses the quadrilateral $(i, j)$. This is a geometric view of the fundamental theorem of phyllotaxis...